



Sea Ice CCI+



ESA CCI+ CLIMATE CHANGE INITIATIVE
PHASE 1: NEW R&D ON CCI ECVs

Contract number:

4000126449/19/I-NB



CCI+ Sea Ice ECV

SEA ICE THICKNESS ALGORITHM

THEORETICAL BASIS DOCUMENT

(ATBD)

Reference: D2.1

Issue: 3.2

Date: 14 September 2023



FMI



Max-Planck-Institut
für Meteorologie

DTU





**Norwegian
Meteorological
Institute**

**The Norwegian Meteorological Institute
(METNO)**

Henrik Mohns Plass 1

N-0313 Oslo

Norway

Phone: + 47 22 96 30 00

Fax: + 47 22 96 30 50

E-Mail: thomas.lavergne@met.no

<http://www.met.no>

Contract

PHASE 1 OF THE CCI+ CLIMATE CHANGE
INITIATIVE NEW R&D ON CCI ECVs

SEA ICE ECV

Deliverable

D2.1 Sea Ice Thickness Algorithm Theoretical
Basis Document

CLIENT

European Space Agency

CLIENT REFERENCE

4000126449/19/I-NB

Revision date:

14 September 2023

Approval date:

27 September 2023

Principal Authors

Stephan Paul, Alfred Wegener Institute

Stefan Hendricks, Alfred Wegener Institute



Eero Rinne, University Centre in Svalbard

Heidi Sallila, Finnish Meteorological Institute

Change Record

Issue	Date	Reason for Change	Author(s)
1.0	29 August 2019	First version	H. Sallila, E. Rinne, S. Hendricks
2.0	29 May 2020	Second version	H. Sallila, E. Rinne, S. Hendricks
2.1	25 June 2020	Response to the RID_D2.1_SIT_v2.0	H. Sallila, E. Rinne, S. Hendricks
3.0	09 June 2021	Third version	S. Paul, H. Sallila, S. Hendricks, E. Rinne
3.1	17 July 2021	Response to the RID_D2.1_SIT_v3.0	S. Paul, H. Sallila, S. Hendricks, E. Rinne
3.2	14 September 2023	Final version	S. Paul, S. Hendricks, E. Rinne, H. Sallila

Document Approval

Role	Name	Signature
Written by:	S. Paul, H. Sallila, E. Rinne, S. Hendricks	
Checked by:	M. A. Killie	
Approved by:	A. M. Trofaier	

Contents

0.1 List of Figures	7
0.2 List of Tables	8
1 INTRODUCTION	9
1.1 Purpose	9
1.2 Scope	9
1.3 Document Status	9
1.4 Acronyms and Abbreviations	9
1.5 Executive Summary	11
2 INPUT AND AUXILIARY DATA	12
2.1 Overview	12
2.2 Primary Altimeter Data Sets	14
2.3 Auxiliary data	15
3 OVERVIEW OF THE SIT PROCESSING CHAIN	17
4 PRE-PROCESSING AND PRIMARY DATA (LEVEL-1 PRE-PROCESSING)	18
4.1 Region Filtering	18
4.2 CryoSat-2 Radar Modes	18
4.3 Orbit Merging	18
4.4 Envisat Backscatter Drift Correction	19
5 GEOPHYSICAL RETRIEVAL (LEVEL-2 PROCESSING)	20
5.1 Orbit Crossovers (XO) and Orbit Trajectory Matches (OTM)	20
5.2 Surface-Type Classification	23
5.2.1 Waveform Parameters	24
5.2.1.1 Radar Backscatter Coefficient	24
5.2.1.2 Pulse Peakiness	24
5.2.1.3 Leading-Edge Width	24
5.2.1.4 Leading-Edge Quality	24
5.2.1.5 Leading-Edge Peakiness	25
5.2.2 Procedure Description	25
5.3 Range Retracking	30
5.3.1 Retracker Thresholds	30
5.3.2 Machine Learning based Sea-Ice Waveform Retracker Threshold	30
5.3.3 Pulse Deblurring	31
5.3.4 Radar Range Uncertainty	31
5.4 Geophysical Range Correction	31
5.5 Sea-Surface Height and Freeboard	32
5.5.1 Sea-Surface Height	32
5.5.2 Sea-Surface Height Uncertainty	32
5.5.3 Freeboard	33
5.5.4 Freeboard Uncertainty	33
5.6 Snow on Sea Ice	35

5.6.1 Snow Depth	35
5.6.2 Snow Depth Uncertainty	38
5.6.3 Snow Density	38
5.6.4 Snow Density Uncertainty	39
5.7 Sea-Ice Thickness	39
5.7.1 Freeboard to Thickness Conversion	39
5.7.2 Sea-Ice Density Uncertainty	40
5.7.3 Sea-Ice Thickness Uncertainty	40
5.7.4 Sea-Ice Type (MYI Fraction) Uncertainty	40
5.8 Filtering	40
5.8.1 General Filters	40
5.8.1 Marginal Ice Zone Filter	42
5.8.1.1 Open-Ocean to Sea-Ice Transition	42
5.8.1.2 Open-Ocean Proximity	43
6 COLOCATION ON SPACE-TIME GRID (LEVEL-3 PROCESSOR)	44
6.1 Grid Temporal Coverage	44
6.2 Grid Spatial Definition	44
6.3 Parameter Gridding	45
6.4 Level-3 Gridded Uncertainties	46
7 GAP INTERPOLATION (LEVEL-4 PROCESSOR)	48
8 SEA-ICE VOLUME COMPUTATION	50
9 REFERENCES	51

0.1 List of Figures

Figure 2-1: Average winter (October to March) Arctic sea-ice thickness in meters from October 1993 to March 2001 computed from pulse-limited ERS satellite altimeter measurements

Figure 2-2: Monthly gridded sea-ice thickness data in the Northern Hemisphere with orbit coverage limits for March 2011 (top panel): Envisat (left) and CryoSat-2 (right) and in the Southern Hemisphere for September 2011 (lower panel)

Figure 2-3: Sea-ice thickness product level examples in both hemispheres. top: Daily orbit trajectories (l2p), bottom: monthly data on space-time grid with different resolution for Northern and Southern Hemisphere

Figure 3-1: Flow chart for the Sea-Ice Thickness Processor

Figure 5-1: Distribution of orbit crossovers (XO) between Envisat and CryoSat-2

Figure 5-2: Distribution of orbit crossovers (XO) between ERS-2 and Envisat

Figure 5-3: Sketches for orbit crossovers (XO) and orbit trajectory matches (OTM)

Figure 5-4: Fractions of classified waveforms in April 2011

Figure 5-5: Surface-type detection fractions for Envisat and CryoSat-2 in April 2011

Figure 5-6: Surface-type detection fractions for Envisat and CryoSat-2 in October 2011

Figure 5-7: Estimation of sea-ice freeboard for one CryoSat-2 orbit segment in April 2014

Figure 5-8: Steps for creating the monthly merged snow depth climatology

Figure 5-9: Regional weight factor for the W99 snow depth climatology

Figure 5-10: Performance example of sea-ice thickness with the merged snow product

Figure 6-1: Gridded uncertainties (Example CryoSat-2 March 2015 Arctic data)

Figure 7-1: Evaluation of CryoSat-2 SIT area averages and their anomalies

Figure 7-2: CryoSat-2 SIT (left); Distance along iceline (DAL; right) for April 2016.

0.2 List of Tables

Table 1-1: Acronyms and Abbreviations

Table 2-1: Summary of used auxiliary data sets

Table 4-1: The table lists the latitudinal boundaries for the Northern and Southern Hemisphere used for the region filtering

Table 5-1: Conditions and waveform parameter thresholds for ERS-2

Table 5-2: Conditions and waveform parameter thresholds for ENVISAT

Table 5-3: Conditions and waveform parameter thresholds for CryoSat-2

Table 5-4: Retracker threshold parametrization for radar range retrieval

Table 5-5: Reference dates for the monthly snow climatology

Table 5-6: List of data filters for Level-2 processing of trajectory based radar altimeter data

Table 5-7: Marginal ice zone (MIZ) filter flag values and meaning

Table 5-8: Marginal ice zone filter scheme for transit from open ocean into the sea ice cover

Table 5-9: Marginal ice zone filter scheme for marginal ice zone passes

Table 6-1: Temporal definition for Level-3 products.

Table 6-2: Projection definition for Level-3 products.

Table 6-3: Grid extent and spacing for Level-3 products.

1 INTRODUCTION

1.1 Purpose

This document is the Algorithm Theoretical Basis for the Sea Ice ECV within CCI+ PHASE 1 - NEW R&D ON CCI ECVs, which is being undertaken by a METNO-led consortium. This document is based on the work of Phase 2 of the ESA CCI project and includes the new developments for the Sea-Ice Thickness (SIT) aspects.

This document also contains preparation and documentation of the ongoing work to extend the CRDP to cover SIT from ERS-1 and ERS-2 satellites as well as for future level-4 products and computation of sea-ice volume. These development items are not completed and will be finalized during CCI+ PHASE 2.

1.2 Scope

The scope of the document is to describe elements of the algorithms that are chosen for implementation during the third and final year of the CCI+ Phase 1, resulting in the production of the CDR. The selected algorithms are presented and justified, but the document does not contain the results of research leading to the selection of these algorithms.

1.3 Document Status

This is the third issue of the ATBD document for the Sea Ice CCI+ project. The document describes the algorithms for the final processing. In addition, the auxiliary data sets used in the initial processing are introduced.

The description of the SIT retrieval algorithm is a combination of the state at the end of the Phase 2 of the SICCI project and the knowledge gained during CCI+ Phase 1. This version differs from the SICCI Phase 2 in that this document contains the added knowledge from ERS-1 and ERS-2 studies, including pulse deblurring correction, as well as the exception of novel snow estimates for the Arctic in areas where Warren climatology is considered outdated. Additionally, the introduction of dual mission orbit crossovers and the added benefit for the current and future CDR production is included in this document. This document is the basis for the produced and published CDR.

1.4 Acronyms and Abbreviations

Table 1-1 below lists the acronyms and abbreviations used in this volume.

Table 1-1: Acronyms and Abbreviations. Acronyms for the deliverable items and partner institutions are not repeated.

Acronym	Meaning
AMSR-E / AMSR2	Advanced Microwave Scanning Radiometer (for EOS / #2)
C3S	EU Copernicus Climate Change Service
CCI	Climate Change Initiative
CDR	Climate Data Record
CS2	ESA's CryoSat-2
DAL	Distance along iceline
DMSP	Defense Meteorological Satellite Program
DMXO	Dual-mission orbit crossover
EASE grid	Equal-Area Scalable Earth Grid
ECMWF	European Centre for Medium-Range Weather Forecasts
ECV	Essential Climate Variable
ENVISAT	ESA's Environmental Satellite
EO	Earth Observation
ERS	European Remote Sensing Satellite
ESA	European Space Agency
EUMETSAT	European Organization for the Exploitation of Meteorological Satellites
FYI	First Year Ice
ICDC	Integrated Climate Data Center
ICDR	Interim Climate Data Record
L1b, L2, L3C, ...	Satellite data processing Level (Level-1b, ...)
LEW	Leading-edge width
MSSH	Mean sea-surface height
MYI	Multi-Year Ice
OSI SAF	EUMETSAT Ocean and Sea Ice Satellite Application Facility
OTM	Orbit trajectory match
PP	Pulse peakiness
RA	Radar Altimeter
RRDP	Round Robin Data Package
S0	Sea-ice backscatter
SIC	Sea-Ice Concentration
SIT	Sea-Ice Thickness
SAR	Synthetic Aperture Radar
SGDR	Sensor Geophysical Data Record
SIRAL	Synthetic Aperture Radar (SAR) Interferometer Radar Altimeter
SMMR	Scanning Multichannel Microwave Radiometer
SMOS	Soil Moisture and Ocean Salinity

SSH	Sea-surface height
SSHA	Sea-surface height anomaly
SSM/I	Special Sensor Microwave/Imager
SSMIS	Special Sensor Microwave Imager/Sounder
TDS	Training data set
W99-AMSR2	The merged Warren-AMSR2 snow climatology
XO	Orbit crossover

1.5 Executive Summary

This document presents the algorithms for producing the Sea Ice Thickness Climate Data Record (SIT CDR) in CCI+. This document can be understood as a recipe book for a software engineer wanting to build a working SIT processor. It also gives the background of used algorithms and data for anyone wanting to understand the CRDP better.

The document includes all the necessary steps for converting altimeter waveforms into sea-ice thickness in along-track (L2), monthly gridded (L3) format, and the gap-free gridded data (L4):

- Filtering data based on latitudes, possibly removing data points based on flags provided with the data
- Introduction and description of the dual-mission orbit crossovers between sensors in their respective mission-overlap periods
- Surface-type classification algorithms based on waveform parameters for differentiating between ocean, lead, sea ice, and ambiguous
- Waveform retracking of the different surface types to obtain ice elevations and sea-surface height tie points over leads between ice floes.
- Application of geophysical range corrections including tidal correction
- Estimation of radar freeboard and along-track sea-surface height from ice surface elevations and interpolated SSH tie points utilizing a mean sea surface
- Radar freeboard to sea-ice freeboard conversion by applying geometric corrections, with snow information
- Sea-ice thickness calculation based on sea-ice freeboard and auxiliary parameters and the assumptions of hydrostatic equilibrium

Along with steps and algorithms, all primary and auxiliary data products used to create the SIT CDR are introduced.

Although the algorithms for the final production are chosen, there are some details that are necessary to be added to the ATBD in its final iteration.

2 INPUT AND AUXILIARY DATA

2.1 Overview

This part of the document is intended as a generic guide to setting up a sea-ice thickness processing system for any polar orbiting satellite radar altimeter. The general method is described and specific examples are given. The general processing system is identical for pulse-limited as well as for SAR altimetry. Any sensor type specific differences are stated.

The method used to extract sea-ice thickness from radar altimetry data is based on the pioneering work of Peacock and Laxon, 2004; Laxon et al., 2003 for the ERS-2 mission. The method involves separating the radar echoes returning from the ice floes from those returning from the sea surface in the leads between the floes. This step of a surface-type classification is crucial and allows for a separate determination of the ice floe and sea-surface heights. The freeboard that is the elevation of the ice upper side (or ice/snow interface) above the sea level can then be computed by deducting the interpolated sea-surface height at the floe location from the height of the floe. Sea-ice thickness can then be calculated from the sea-ice freeboard with the additional information of the snow load. **Figure 2-1** shows an example of the earliest results of Laxon et al. (2003) with aggregated ERS data. **Figure 2-2** and **Figure 2-3** show the progression in terms of spatial and temporal resolution of altimeter-based sea ice thickness information with the extension to the Envisat and CryoSat-2 platforms in the ESA CCI project since the first application of the method.

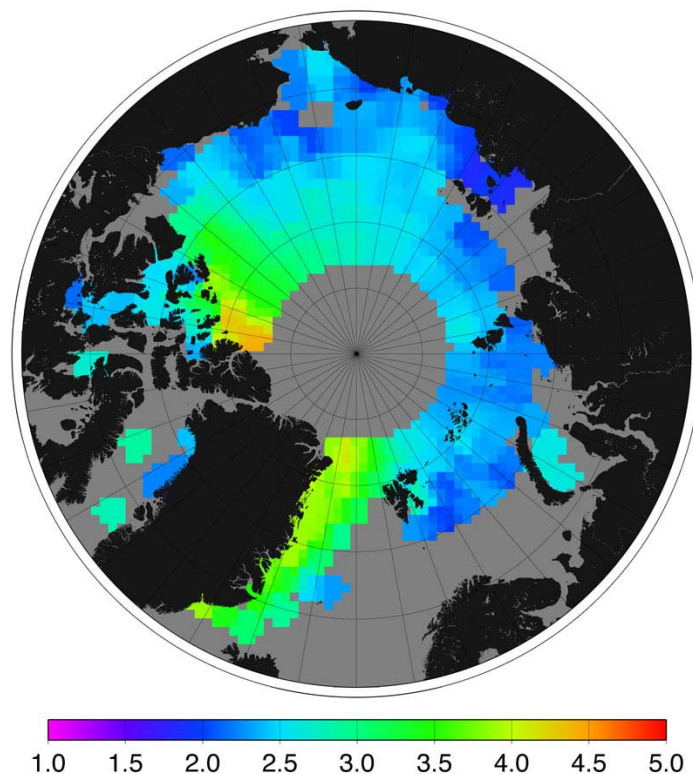


Figure 2-1: Average winter (October to March) Arctic sea-ice thickness in meters from October 1993 to March 2001 computed from pulse-limited ERS satellite altimeter measurements.

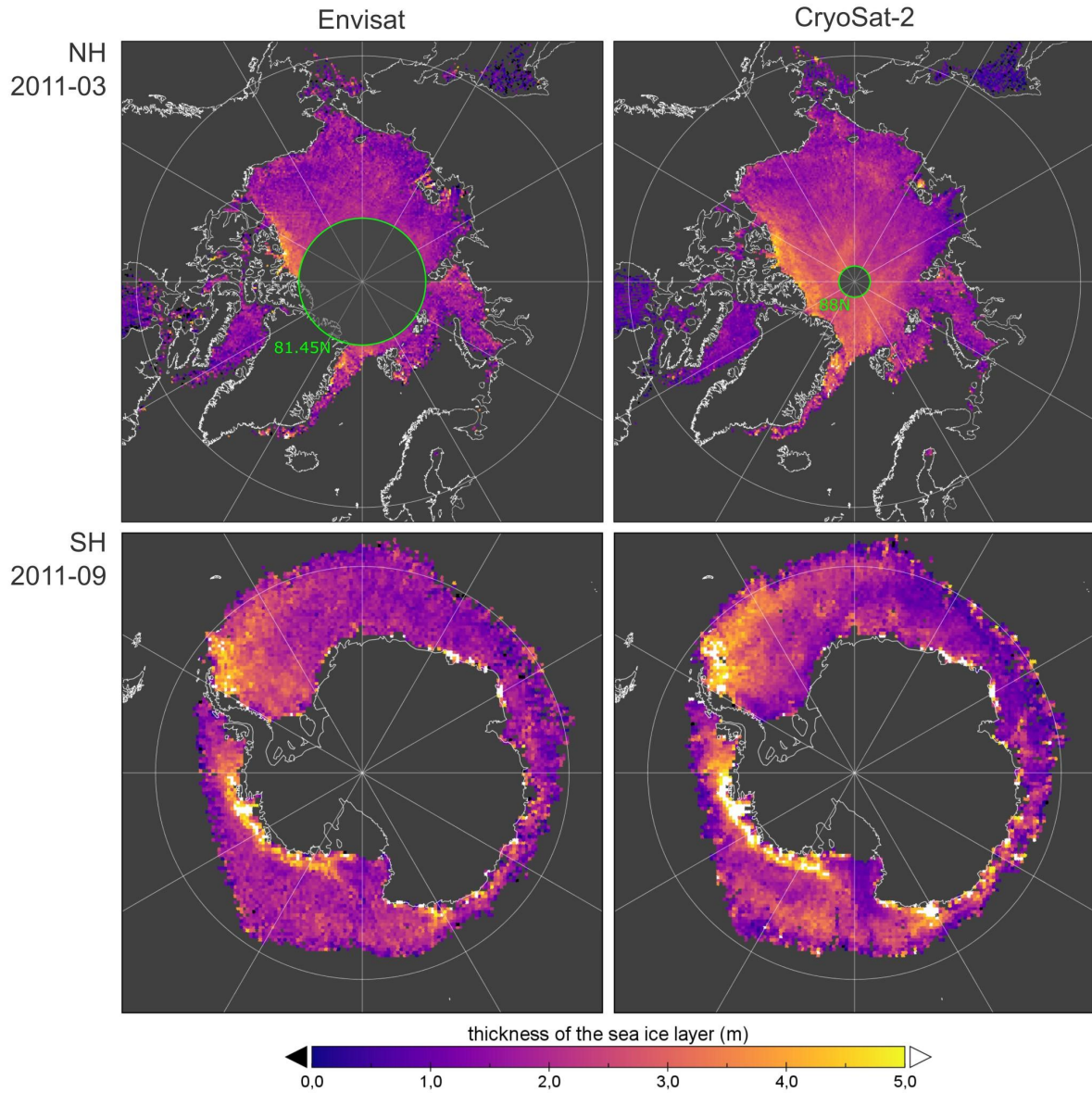
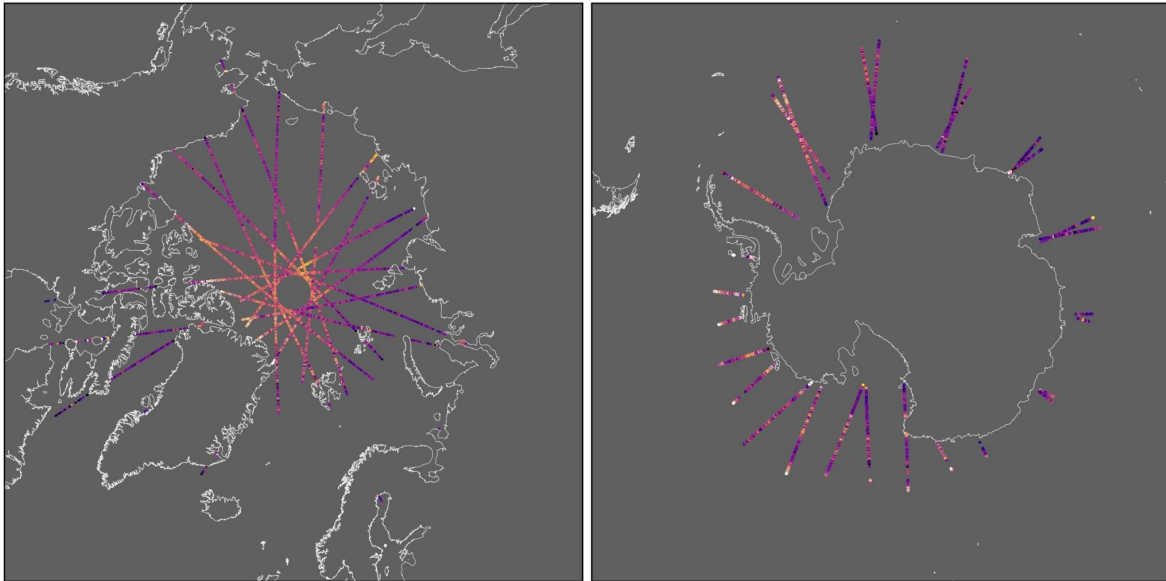


Figure 2-2: Monthly gridded sea ice thickness data in the Northern Hemisphere with orbit coverage limits for March 2011 (top panel): Envisat (left) and CryoSat-2 (right) and in the Southern Hemisphere for September 2011 (lower panel)

Level 2 (L2P): Daily orbit trajectories



Level 3 (L3C): Monthly gridded fields (Arctic: 25 km, Antarctic: 50 km)

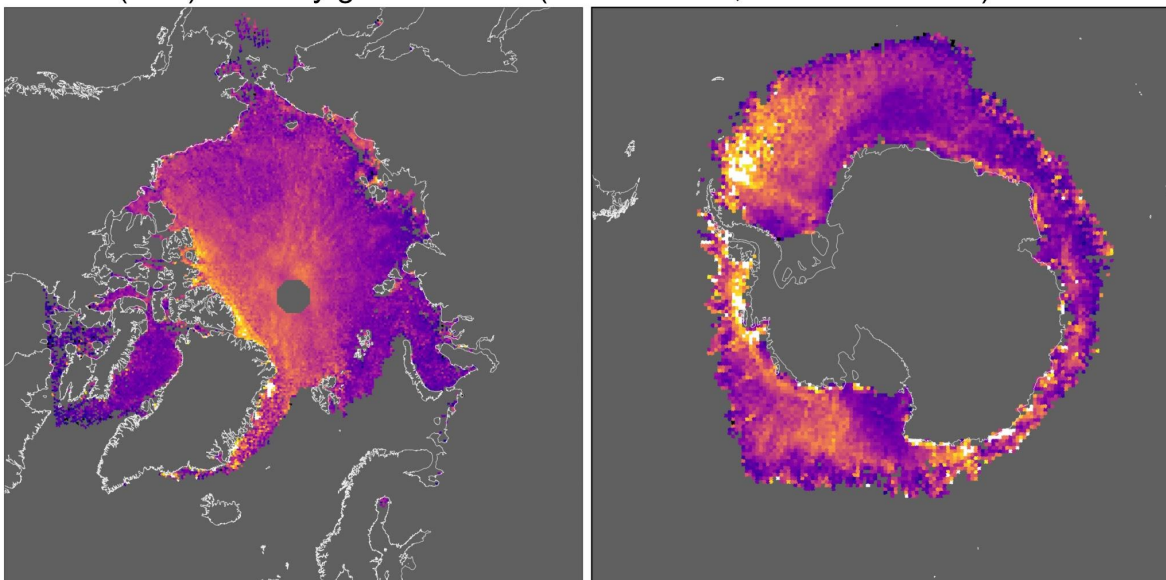


Figure 2-3: Sea-ice thickness product level examples in both hemispheres. top: Daily orbit trajectories (l2p), bottom: monthly data on space-time grid with different resolution for Northern and Southern Hemisphere.

2.2 Primary Altimeter Data Sets

The input data set must contain the radar echo waveforms and all other fields mentioned in this document such as altitude, range, atmospheric corrections and geophysical corrections. Figure 3-1 shows a flow chart for each step of the sea-ice thickness processor. Each step is

explained in detail in the sections below. For ERS-1 and ERS-2 RA the REAPER Sensor Geophysical Data Record (SGDR) data (Brockley et al., 2017) is used. In the case of Envisat RA-2, the input for the sea-ice thickness processor is version 3.0 of the Envisat SGDR data (ESA, 2018). The SGDR data contains the waveforms as well as all other required fields. The ERS data is provided per cycle files or daily files. For Envisat data, each orbit is stored in two data files. The earlier of the two data files contains the data for the ascending arc from -81.5 latitude up to +81.5 latitude, and the later of the two the descending arc from +81.5 latitude back down to -81.5 latitude. These files are read sequentially and the output split at appropriate points to make continuous Arctic and Antarctic passes.

For CryoSat-2, the version 1.0 of Baseline D orbit data files are used and separated into sections of different instrument modes by the processor. CryoSat-2's SIRAL altimeter is operated in two different modes over sea ice: a) In synthetic aperture radar (SAR) off-coast and b) in synthetic aperture radar interferometric (SIN) mode to enable more accurate land ice altimeter measurements with higher surface slopes. For the product generation both radar modes are used, but the processing does not utilize the interferometric information in SIN mode. In addition to the different altimeter type that improves the spatial resolution, the higher orbit inclination of CryoSat-2 allows sea-ice thickness measurements in the Arctic up to 88N.

2.3 Auxiliary data

The conversion into sea-ice freeboard requires either the use of auxiliary input data or a parametrization of snow depth. For the Arctic, where in SICCI Phase 2 only Warren climatology (W99, Warren et al., 1999) was applied, we now use a merged Warren-AMSR2 (W99-AMSR2) snow climatology for all the instruments, further described in Section 5.5. One main reason for the change is that the Warren climatology is based on data sets obtained from Arctic drift stations in regions of multi-year sea ice (MYI), snow depth values are suspected to be biased high over first-year sea-ice (FYI).

In order to discriminate between FYI and MYI in the Arctic, we resort to Copernicus Climate Change Service (C3S) Climate Data Record (CDR)/interim-CDR (ICDR). In SICCI Phase 2 a MYI fraction data set based on the Special Sensor Microwave Imager (SSM/I)/Special Sensor Microwave Imager Sounder (SSMIS) sensors on-board of the Defense Meteorological Satellite Program (DMSP) satellites provided by the Integrated Climate Data Center (ICDC) was used. The C3S CDR is produced with an algorithm that is optimized to produce consistent CDRs based on time series of passive microwave data of the above-mentioned instruments, in addition with SMMR and ECMWF ERA-Interim data.

Table 2-1: Summary of used auxiliary data sets.

Parameter	ERS-1 /2 Arctic	ERS- 1 / 2 Antarctic	Envisat RA-2 Arctic	Envisat RA-2 Antarctic	CryoSat-2 Arctic	CryoSat-2 Antarctic
SIC	C3S CDR	C3S CDR	C3S CDR	C3S CDR	C3S CDR/ICDR	C3S CDR/ICDR
SIType	C3S CDR	Single Ice Type	C3S CDR	Single Ice Type	C3S CDR/ICDR	Single Ice Type
Snow Depth	Merged W99-AMSR2 climatology	AMSR-e climatology	Merged W99-AMSR2 climatology	AMSR-E/2 climatology	Merged W99-AMSR2 climatology	AMSR-E/2 climatology
Snow Density	Mallett et al., 2020	fixed/clim	Mallett et al., 2020	fixed/clim	Mallett et al., 2020	fixed/clim
MSS	DTU21	DTU21	DTU21	DTU21	DTU21	DTU21

For the Antarctic, we assume only a single sea-ice type being present. As the Warren climatology is only available for the Arctic, we use a snow-depth climatology derived from the Advanced Microwave Scanning Radiometer-EOS (AMSR-E) and AMSR-2 data for the Antarctic. This data set is based on a revised version of the approach described by Cavalieri et al. (2014) and provided by the ICDC.

Other required auxiliary input data sets for the estimation of sea-ice freeboard and sea-ice thicknesses comprise the use the sea-ice concentration (SIC) data obtained from the C3S CDR for both hemispheres, in contrast to the SIC product from Ocean and Sea Ice Satellite Application Facility (OSISAF) used in SICCI Phase 2. For mean sea-surface (MSS) height the product provided by the Danish Technical University (DTU) in its 2021 version is used.

A summary of all used auxiliary data sets for the production of the sea-ice thickness climate data record is presented in **Table 2-1**.

3 OVERVIEW OF THE SIT PROCESSING CHAIN

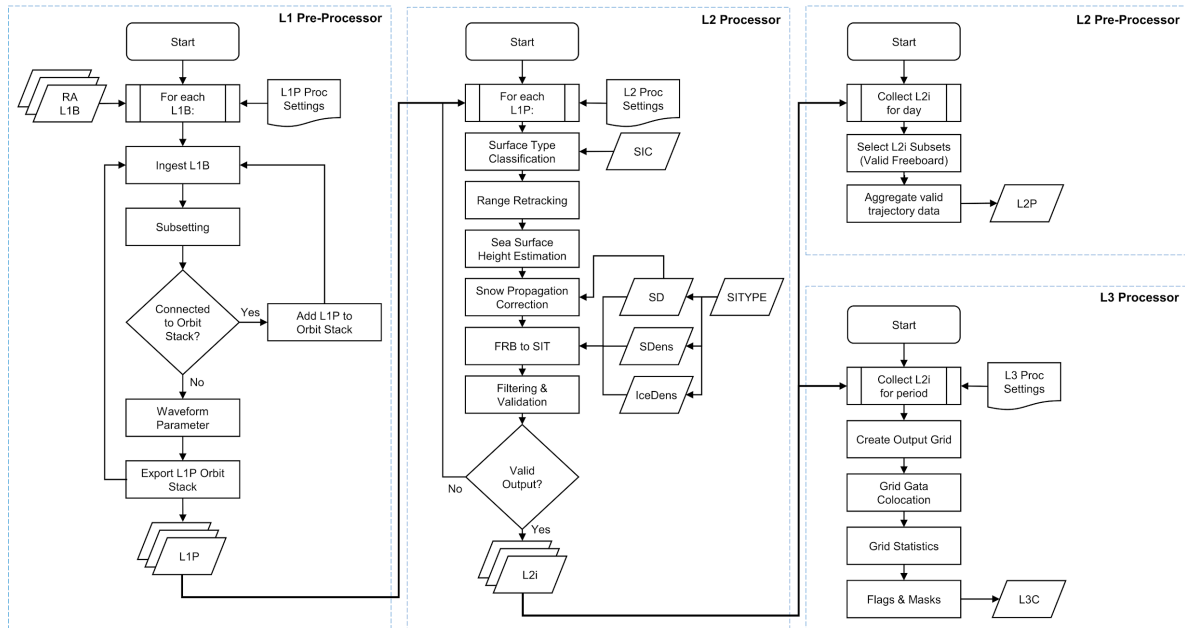


Figure 3-1: Flow chart for the Sea-Ice Thickness Processor

Figure 3-1 presents an overview about the sea-ice thickness processing chain detailed into defined processors for the successive product data levels. The structure of the following sections is modeled after these processors that include details for each sensor. The geophysical retrieval starts with the surface-type classification, with the corresponding parametrization for ERS-1 and ERS-2, Envisat and CryoSat-2. This continues with a thorough description of the range retracking procedure and a necessary Envisat RA-2 backscatter correction. Furthermore, the processing chain of radar freeboard and sea-surface height derivation, the estimation of sea-ice freeboard, and the estimation of sea-ice thickness are described. The subsections contain the computation of the geophysical parameters as well as the corresponding uncertainties.

While the geophysical retrieval is implemented at full sensor resolution, the aggregation of the parameter to space-time grids is described in the following sections of this document.

The processors are implemented in the python sea-ice radar altimetry toolbox (pysiral). This open source software project is hosted at Github (<https://github.com/pysiral/pysiral>) and allows the inspection of the actual implementation of all algorithm components.

4 PRE-PROCESSING AND PRIMARY DATA (LEVEL-1 PRE-PROCESSING)

The main purpose of the pre-processing of the primary level-1 data is to provide a unified input format and data conventions for the following geophysical retrieval.

4.1 Region Filtering

The latitudinal boundaries within which Arctic and Antarctic sea ice is found are listed in **Table 4-1**. The latitude values in the satellite data are examined and any data points outside these regions are rejected from the processing. The surface-type flag in the data is also examined and any data not flagged as over ocean is also rejected.

Table 4-1: The table lists the latitudinal boundaries for the Northern and Southern Hemisphere used for the region filtering

Area	Minimum Latitude	Maximum Latitude
Arctic	45.0	90.0
Antarctic	-90.0	-45.0

The data is cropped to the two latitude ranges and data over land masses are excluded, except if the orbit segment over land is shorter than 300 km. Else, the orbit is split into two segments.

4.2 CryoSat-2 Radar Modes

Only for CryoSat-2, the altimeter data is divided into orbit segments in three radar modes: LRM, SAR and SARIn. Of these we disregard LRM due to its little relevance over sea ice, thus using only SAR and SARIn modes. These come in separate product files, which are merged in the pre-processor. The merging process requires reducing the SIN waveforms from 512 to 256 range bins of the SAR waveforms. This can be done without losing waveform information as the sea-ice waveforms are narrow and defined. The step is unique to CryoSat-2, as other platforms (ERS-1/2, Envisat) provide data only with a single radar mode.

4.3 Orbit Merging

Adjacent neighboring orbit segments are merged into a single orbit segment over the polar regions whenever possible to enable consistent sea-surface height estimation across the Arctic polar basin. Due to the geography in the Antarctic, the descending and ascending orbit segments over the ocean will always be separated by the Antarctic continent.

4.4 Envisat Backscatter Drift Correction

Over the course of Envisat's life span, it appears that the RA-2 instrument has been degraded. This results in a slight linear reduction in received backscatter over the years (**Figure 4-1**). As this can affect both the surface-type classification as well as the range retracking (as both are dependent on the received sea-ice backscatter), a correction had to be applied.

The monthly degradation factor of -0.003269253 was derived from the monthly averages of ocean-type waveforms in the Barents Sea (70°N-75°N and 40°E-50°E). Ocean-type waveforms are derived independent from the sea-ice backscatter classifier and we assume the surface roughness sufficiently random compared to ice-type waveforms for this type of analysis.

Instead of correcting all backscatter values to the original baseline, the earlier backscatter data was adjusted to the levels of the center month (June 2011) of the CryoSat/Envisat overlap period with the following function:

$$t_{sift} = 12 \times (\alpha_{ref} - \alpha) + (m_{ref} - m)$$

$$\sigma_{drift}^0 = -0.003269253 \times t_{sift}$$

Here, t_{sift} is the time shift factor in months between the reference year (a_{ref}) and month (m_{ref}) and the currently processed year (a) and month (m). The resulting backscatter drift correction σ_{drift}^0 is then added to the sea-ice backscatter before the surface-type classification and the range retracking. By doing so, the in general slightly higher backscatter values during earlier years of Envisat's lifespan are reduced to the level during the sensor overlap period.

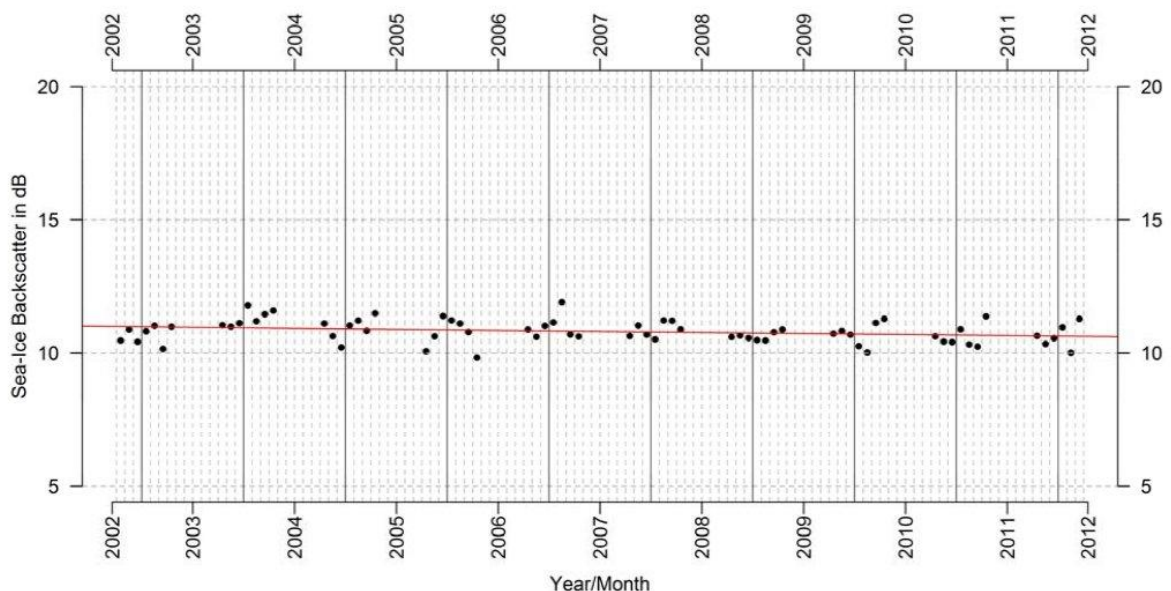


Figure 4-1: Visualizations of the monthly averaged sea-ice backscatter reduction between 2002 and 2012 over ocean-type waveforms obtained between 70°N-75°N and 40°E-50°E

5 GEOPHYSICAL RETRIEVAL (LEVEL-2 PROCESSING)

The level-2 processing step includes the retrieval of the geophysical variables from the pre-processed radar measurements, with the use of auxiliary data listed in **Table 2-1**.

5.1 Orbit Crossovers (XO) and Orbit Trajectory Matches (OTM)

The basis for the retracker tuning of Envisat RA-2 as well as the surface-type classification, are dual mission orbit crossovers (XO). All XOs utilize waveforms acquired per sensor within a 12.5 km radius around the actual orbit crossover in the central Arctic and the marginal seas East of 70°E and West of 95°W and above a latitude of 70°N (**Figure 5-1**). For the best possible results, all analysis are limited to XOs that occurred within a maximum time difference of twelve hours.

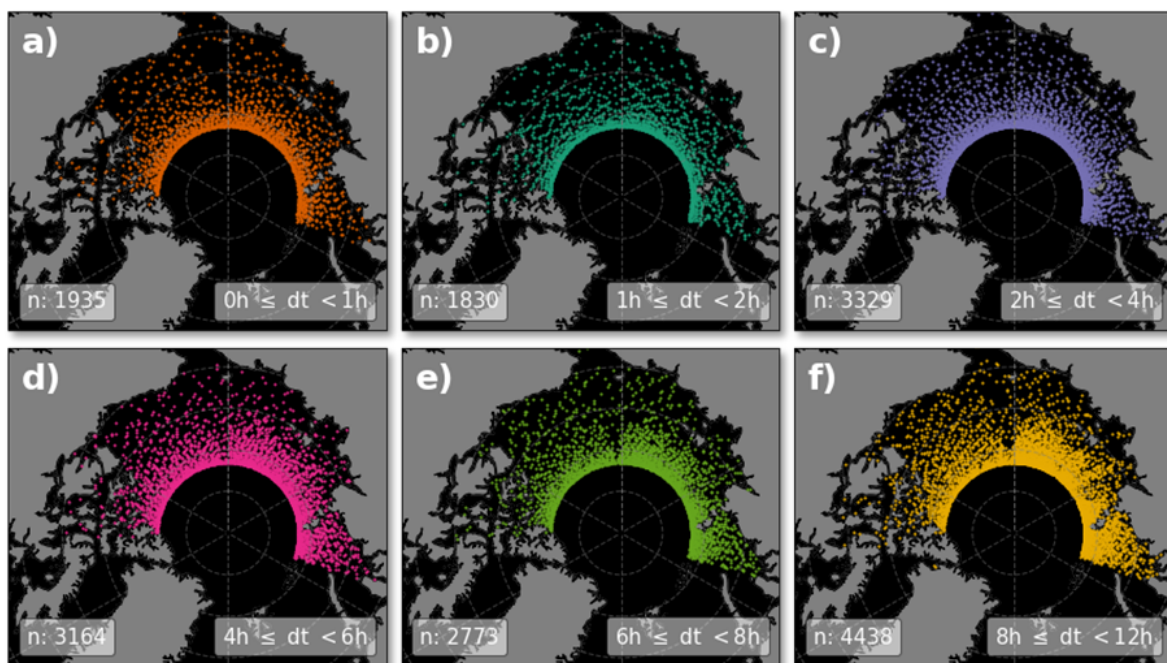


Figure 5-1: Distribution of orbit crossovers (XO) between Envisat and CryoSat-2 between October 2010 and April 2012 for various crossing time differences (dt).

Based on the examples shown in **Figure 5-1**, this results in roughly 17.000 XOs within a 12 hours time difference for the respective mission overlap period.

While XOs work well for the CryoSat-2/ENVISAT overlap, due to different orbit configurations their use is limited for any ERS/ENVISAT overlap (**Figure 5-2**). However, both missions flew on an almost similar orbit with a minimum time difference allowing for the investigations of waveform differences in so-called orbit trajectory matches (OTM) using a buffer of 1.5 km around each ERS-2 waveform to collect Envisat waveforms to compare it to. Schematics for both types, XO and OTM, are shown in **Figure 5-3**.

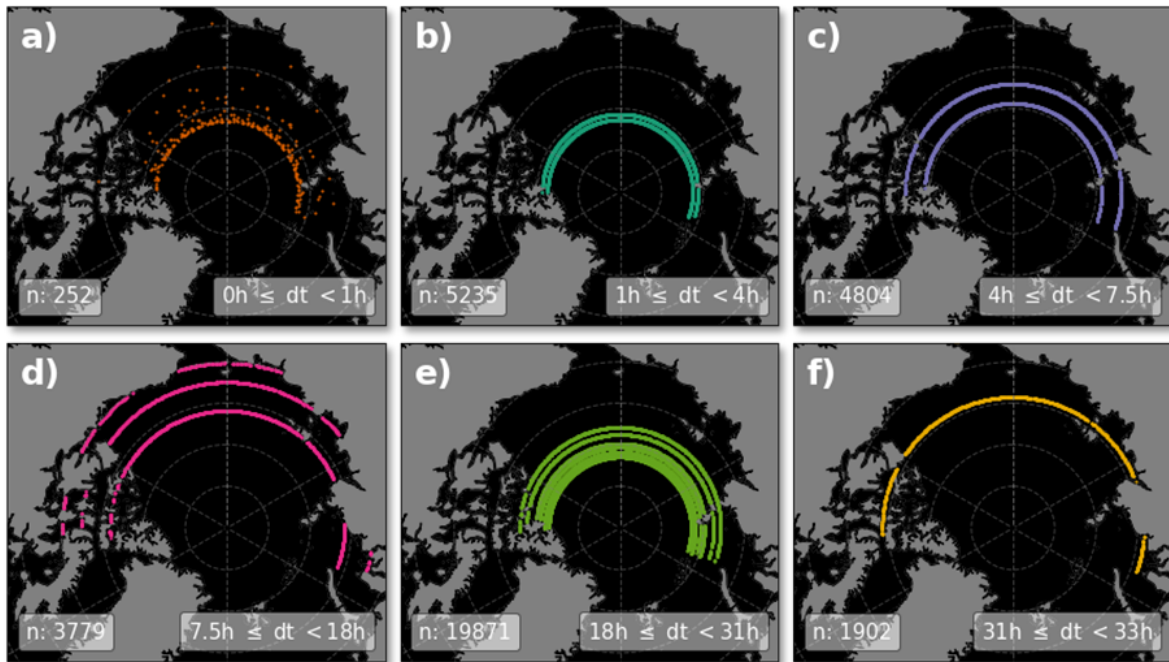


Figure 5-2: Distribution of orbit crossovers (XO) between ERS-2 and Envisat between October 2002 and April 2003 for various crossing time differences (dt).

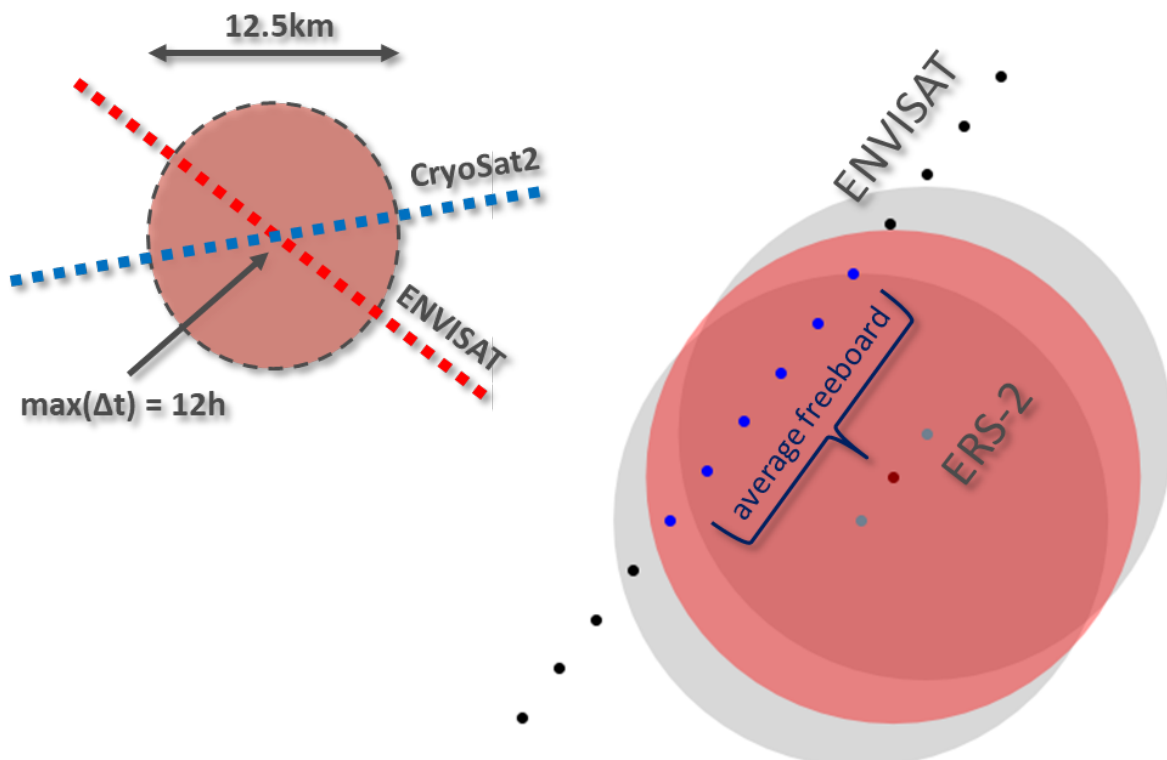


Figure 5-3: Sketches for orbit crossovers (XO, left) and orbit trajectory matches (OTM, right) between CryoSt-2/Envisat and ERS-2/ Envisat, respectively.

Working with these XO/OTMs allows for a i) more detailed investigation into waveform parameters while at the same time reducing limitations of current implementations, as well as ii) a more direct possibility to tune (and retune) older sensors to CryoSat-2 whenever necessary as the data basis is reduced compared to the full available data record of all sensors.

For the generation of the training data set (TDS), both L1p and L2i are used, i.e. the waveforms as well as freeboard estimates per 1% threshold step between 10% and 99% of the first-maximum-index power of each individual waveform. In total, this summarizes the normalized waveform power per range bin and waveform as well as the waveform parameters of radar backscatter, pulse peakiness, and leading-edge width/peakiness/quality. All of these are further described in the following sections.

The key part of the TDS are the labels generated for each waveform, the optimal-retracker thresholds. The initial data cleanings and computation of the optimal-retracker thresholds for the CryoSat-2/ENVISAT overlap comprises the following steps:

1. Elimination of all non-sea-ice-type waveforms from further processing
2. Exclusion of XO's with less than 15 remaining sea-ice waveforms from either sensor
3. Calculation of the average CryoSat-2 freeboard per XO (**Figure 5-3**)
4. Calculation of the absolute freeboard difference between each individual ENVISAT waveform for each retracker threshold step between 10% and 99% of the first-maximum-index power and the computed average freeboard per XO
5. Identification of the threshold with the lowest absolute freeboard difference per individual waveform and it's assignment as optimal-retracker threshold
6. Exclusion of all values that have an absolute freeboard difference above 1.5 cm on both end of the threshold spectrum

While similar in general, the data cleaning and computation of optimal-retracker thresholds differs for the OTM's by comprising the following steps:

1. Elimination of all non-sea-ice-type waveforms from further processing
2. Computation of 1.500 m buffers around each ERS-2 waveform footprint and extraction of intersecting ENVISAT waveform footprints (**Figure 5-3**)
3. Calculation of the average ENVISAT freeboard per ERS-2 buffered waveform footprint
4. Calculation of the absolute freeboard difference between each individual ERS-2 waveform for each retracker threshold step between 10% and 99% of the first-maximum-index power and the computed average freeboard per ERS-2 buffered waveform footprint
5. Identification of the threshold with the lowest absolute freeboard difference per individual waveform and it's assignment as optimal-retracker threshold

6. Exclusion of all values that have an absolute freeboard difference above 0.5 cm on both end of the threshold spectrum

The TDS compiled from all XO/OTMs is the basis for all machine-learning based training for the range retracking as well as the foundation for any threshold derivations for the surface-type classification. Details shall be provided in the respective sub sections.

5.2 Surface-Type Classification

The surface-type classification is a crucial part in the processing chain of deriving sea-ice freeboard (and therefore sea-ice thickness), as the detection of leads is pivotal for determining the sea-surface height. The sea-surface height in turn is used as the reference from which the sea-ice freeboard is calculated. Additionally, a clear distinction between leads, sea ice and ambiguous mixed signals (which will be excluded from the actual freeboard retrieval) helps to improve the quality and accuracy of resulting sea-ice freeboard estimates. In other words, a surface-type selection bias is very likely to also have an impact on the resulting sea-ice freeboard and hence also the sea-ice thickness and subsequent products.

For the surface-type classification, four different surface types are considered:

1. Open ocean areas. Currently not used.
2. Leads and other openings between ice floes used for sea-surface height estimation.
3. Sea-ice surface used for freeboard and thickness retrieval.
4. Mixed surface/unknown that are discarded from further processing.

The classification is based on five parameters that describe the waveform shape and have distinct properties for waveforms over leads and ice surfaces:

1. Radar backscatter coefficient (SIG0),
2. Pulse peakiness (PP),
3. Leading-edge width (LEW),
4. Leading-edge peakiness (LEP), and
5. Leading-edge quality (LEQ).

These waveform parameters together with the sea-ice area mask (based on the sea-ice-concentration auxiliary data) are used in the procedure and further described in the following sections.

5.2.1 Waveform Parameters

5.2.1.1 Radar Backscatter Coefficient

The radar backscatter coefficient describes the reflectivity of the surface and is strongly related to the maximum power of the waveform.

5.2.1.2 Pulse Peakiness

The pulse peakiness (pp) parameter follows the definition of Ricker et al. (2014):

$$pp = \sum_{i=1}^{N_{wf}} \frac{\max(wf)}{wf_i} \cdot N_{wf}$$

Where:

wf is the radar altimeter waveform,

wf_i is the i th element of the waveform, and

N_{wf} is the number of range bins (data records) of the radar altimeter waveform.

5.2.1.3 Leading-Edge Width

The leading-edge width is defined as the width in range bins along the power rise to the first maximum between 5% and 95% of the peak power while using a ten-time oversampled waveform.

5.2.1.4 Leading-Edge Quality

The leading-edge quality (leq) parameter is used to assess if the leading edge is impacted by noise or other artifacts. The parameter is defined as the ratio between the power at the index of the first maximum (FMI) to the cumulative power rise towards this point.

$$leq = \frac{\sum_{i=2}^{fmi} (wf_i - wf_{i-1})}{wf_{fmi}}$$

Where:

wf is the radar altimeter waveform,

wf_i is the i th element of the waveform, and

fmi is the index of the first maximum

If the ratio is 1, the leading edge has a strictly monotonous increase. An upper limit for lep limits the use of waveforms with a noisy leading edge that would negatively impact retracker range.

5.2.1.5 Leading-Edge Peakiness

The leading-edge peakiness (lep) parameter also follows the definition of Ricker et al. (2014) for what they called the ‘left’ pulse peakiness:

$$lep = \sum_{i=1}^{N_{wf}} \frac{\max(wf)}{\text{mean}([wf_{i_{max}-3} - wf_{i_{max}-1}]])} \cdot 3$$

Where:

wf is the radar altimeter waveform,

$wf_{i_{max}}$ is the i th element of the waveform with the first maximum.

5.2.2 Procedure Description

Classification parameters are used for all radar altimeter platforms (ERS, ENVISAT, CryoSat-2) to classify the surface types of ocean, leads and sea ice. In the case for CryoSat-2, this is done for each radar mode (SAR, SIN & LRM). All waveforms that are not in any of these categories are labeled as unknown and are discarded from further use.

The classification workflow is as follows:

1. Classification of ocean waveforms based on sea-ice mask.
2. Classification of lead waveforms based on sea-ice mask and waveform parameters.
3. Classification of sea-ice waveforms based on sea-ice mask, waveform parameters and the lead classification.
4. Labeling remaining waveforms as unknown.

The classification only depends on the sea-ice mask and the waveform parameters. The thresholds for sea-ice concentration and waveform parameters are listed in **Table 5-1** for ERS-2, **Table 5-2** for Envisat, and **Table 5-3** for CryoSat-2. An exemplary (best case scenario) fraction of either ocean, lead, or sea-ice waveforms in relation to the total number of waveforms for Envisat and CryoSat-2 are shown in **Figure 5-4**. Classification results for both platforms are shown for March 2011 (**Figure 5-5**) and October 2011 (**Figure 5-6**). The two cases are considered to be exemplary for sea-ice conditions at the end and beginning of an Arctic Winter season.

Table 5-1: Conditions and waveform parameter thresholds for ERS-2 pulse limited waveforms to be classified as surface types of ocean, lead and sea ice.

Surface Type	Parameter	Condition
Ocean	Sea-Ice Concentration	< 15%
Lead	Sea-Ice Concentration	> 15%
	PP	> 15.42
	SIG0	> 19.23
	LEW	< 0.94
Sea Ice	Sea-Ice Concentration	> 15%
	PP	> 4.64
	SIG0	> 12.72
	LEW	> 0.84 & < 1.10
	LEP	> 9.92
	LEQ	< 1.0008
	Surface Type	is not class Lead

Table 5-2: Conditions and waveform parameter thresholds for ENVISAT pulse limited waveforms to be classified as surface types of ocean, lead and sea ice.

Surface Type	Parameter	Condition
Ocean	Sea-Ice Concentration	< 15%
Lead	Sea-Ice Concentration	> 15%
	PP	> 26.0
	SIG0	> 25.0
	LEW	< 0.82
Sea Ice	Sea-Ice Concentration	> 15%
	LEQ	< 1.02
	Surface Type	is not class Lead

Table 5-3: Conditions and waveform parameter thresholds for CryoSat-2 waveforms to be classified as surface types of ocean, lead and sea ice. CryoSat-2 provides

waveforms in three radar modes (SAR, SIN, LRM) requiring adapted surface-type classification thresholds for each radar mode.

Surface Type	Parameter	Condition SAR	Condition SIN	Condition LRM
Ocean	Sea-Ice Concentration	< 15%	< 15%	< 15%
Lead	Sea-Ice Concentration	> 15%	> 15%	N/A
	PP	> 66.0	> 260.0	N/A
	SIG0	> 23.0	> 24.0	N/A
	LEW	< 0.75	< 1.05	N/A
Sea Ice	Sea-Ice Concentration	> 15%	> 15%	N/A
	LEQ	< 1.02	< 1.02	N/A
	Surface Type	is not class Lead	is not class Lead	N/A

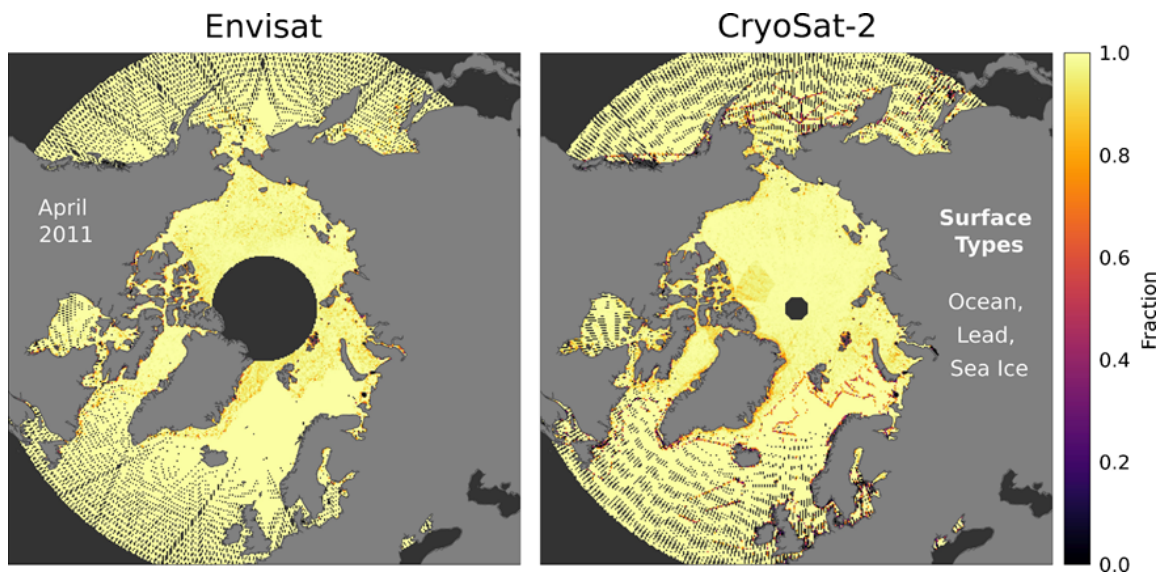


Figure 5-4: Fractions of waveforms that are classified as either ocean, lead or sea-ice waveforms in April 2011. Values smaller than 1 indicate the presence of waveforms classified as `unknown`.

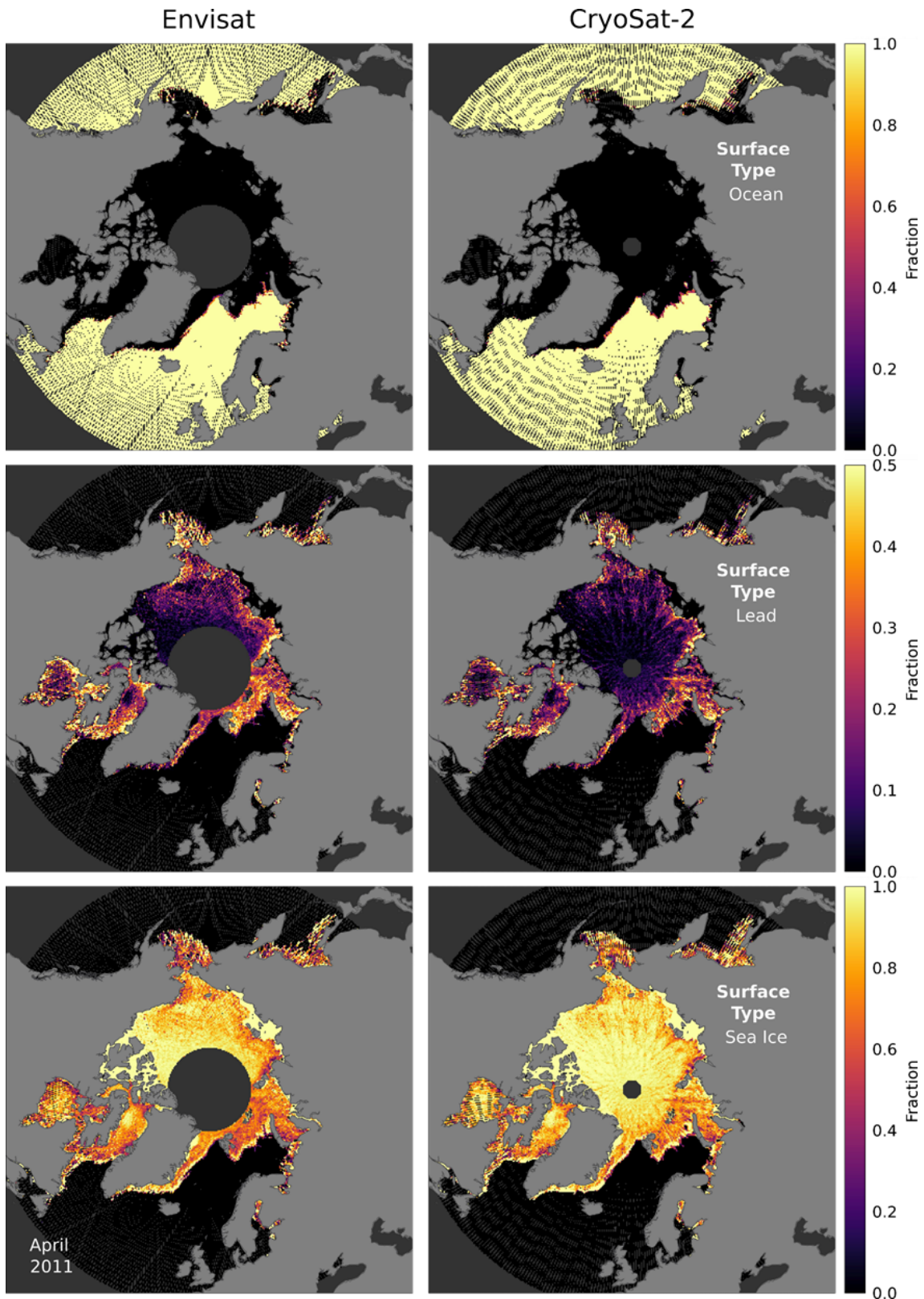


Figure 5-5: Surface-type detection fractions per grid cell for Envisat (left panels) and CryoSat-2 (right panels) in April 2011 at the end of the Arctic Winter Season. From top to bottom: Ocean waveforms, lead waveforms and sea-ice waveforms. The sum of all fractions is 1 for each grid cell.

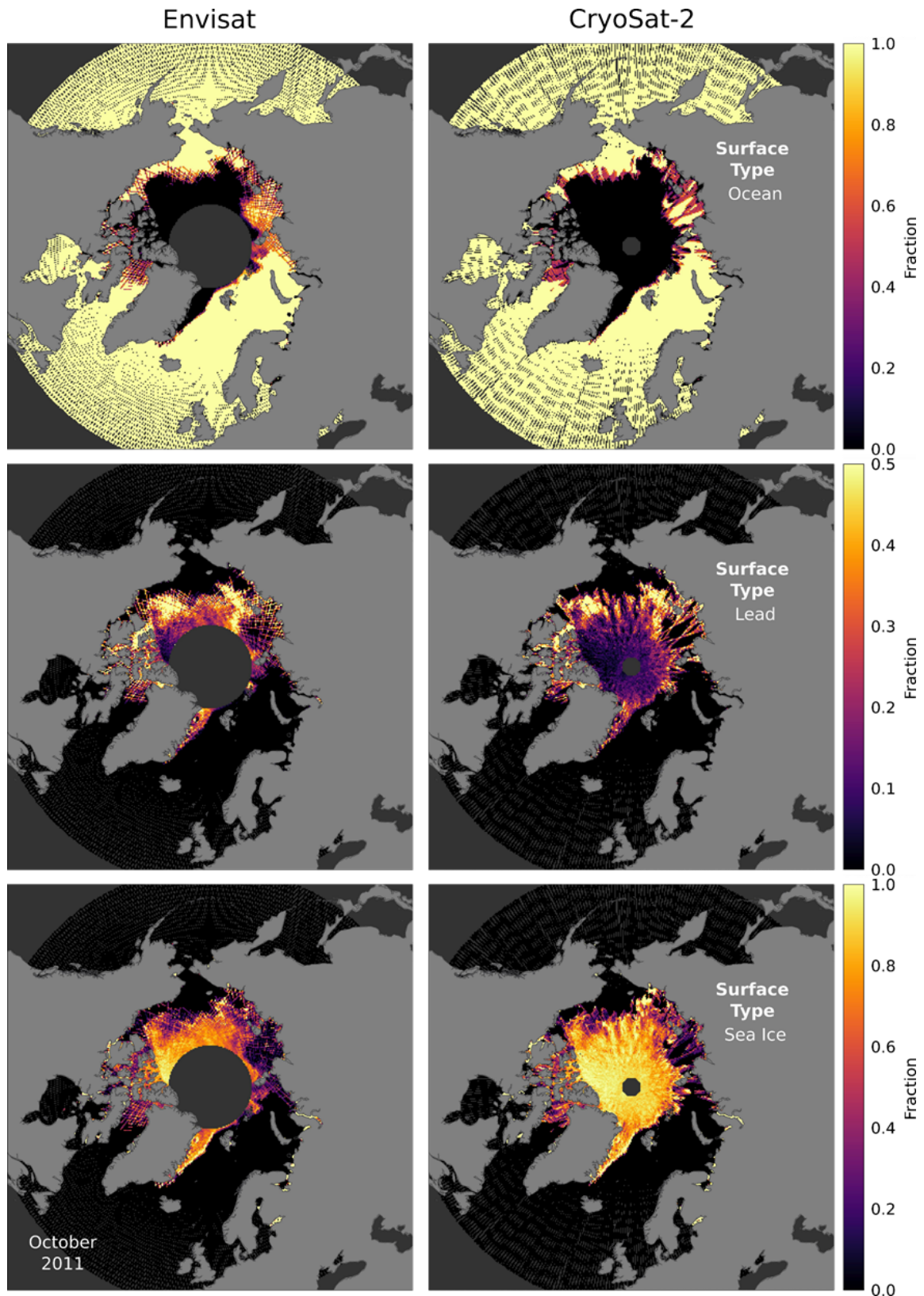


Figure 5-6: Surface-type detection fractions per grid cell for Envisat (left panels) and CryoSat-2 (right panels) in October 2011 at the start of Arctic winter season. From top to bottom: Ocean waveforms, lead waveforms and sea-ice waveforms. The sum of all fractions is 1 for each grid cell.

All thresholds were derived based on the XO/OTMs derived TDS by unsupervised clustering using a mini-batch k-means approach based on 25 clusters and manually identifying lead-type waveforms. All these lead-type clusters were then merged and the thresholds derived by using the 5%/10% percentile for minimum thresholds as well as the 90%/95% percentile for maximum thresholds for each waveform parameter of this cluster stack.

5.3 Range Retracking

5.3.1 Retracker Thresholds

An implementation of the Threshold First Maximum Retracker Algorithm (TFMRA, Helm et al. 2014, Ricker et al, 2014) is used to estimate the range to the main scattering horizon for each waveform of each sensor. The sub-waveform retracker estimates the range, by computing the time where the power of the smoothed leading edge has risen to a defined percentage of the peak power value. The percentage of the peak power, or retracker threshold, varies with surface type and between radar type (pulse-limited waveforms for Envisat and Doppler-delay waveforms for CryoSat-2). A summary of the used retracker thresholds is given in **Table 5-4**.

Table 5-4: Retracker threshold parametrization for radar range retrieval over lead and ice surfaces

	Lead Waveforms	Sea-ice Waveforms
ERS-2	95%	Computed (see below)
Envisat	95%	Computed (see below)
CryoSat (SAR/SIN)	50%	50%

5.3.2 Machine Learning based Sea-Ice Waveform Retracker Threshold

In the case of ERS and Envisat pulse-limited waveforms, the in general lower range-bin resolution as well as the larger impact of sea-ice surface roughness on the leading edge does not allow a fixed retracker threshold to be defined. The retracker threshold is therefore determined from the waveform shape using a machine-learning (ML) approach that slightly differs between the sensors.

The estimation of the sea-ice retracker threshold is based on a feed-forward artificial-neural-network approach, which is trained using estimated optimal-retracker thresholds for intermission orbit crossovers (XO; between CryoSat-2 and Envisat) and subsequently for intermission orbit trajectory matches (OTM; between Envisat and ERS-2) as described in Section 5.1.

Here, the trained network computes a retracker threshold solely on a 35-bin (Envisat/ERS-2) or 45-bin (CryoSat-/Envisat) subset of the received and normalized echo waveform. These subsets are built around the identified first-maximum index (FMI) using 5 bins before and 30

bins after it for ERS-2/Envisat as well as 10 bins before and 35 bins after it for CryoSat-2/Envisat. This approach is independent from any auxiliary data or associated waveform parameters and solely relies on the normalized echo power of each individual waveform. The model files and configurations used to estimate sea-ice retracker threshold are publicly available (Paul and Hendricks, 2022, Paul and Hendricks, 2023).

5.3.3 Pulse Deblurring

A significant challenge in ERS retracking is the pulse blurring which results from the range window moving during waveform averaging sequence, causing short wavelength noise in the retracked elevations. For a detailed description of pulse blurring, see Peacock and Laxon (2004). Due to a strong linear trend between the height error signal ε and the retracked elevation, a correction can be applied to the elevation measurements as a function of ε . A linear correction to the retracked range is applied if the height error signal $\varepsilon < 0$. We utilize the `htl_disc_out` variable from the REAPER SGDR files, convert this into ε in meter and apply the correction as introduced in Peacock (1998), and revisited in ESA (2021):

$$h_{corr} = h_{rtk} - \frac{\varepsilon}{m}$$

where h_{corr} is the corrected height calculated from the retracked height h_{rtk} , HTL error signal ε and slope of the trend m . The slope term is assumed to be constant for all ε , and based on simulations of Peacock (1998) it is -3.5 for ERS-1 and -5.0 for ERS-2.

5.3.4 Radar Range Uncertainty

The uncertainty for the range retrieval and the surface elevation for each waveform is parametrized as fixed values for each sensor (ERS-2: 15cm, Envisat: 15cm, CryoSat-2: 10cm).

5.4 Geophysical Range Correction

The TFMRA returns a time that is converted into range by assuming vacuum light speed as wave propagation velocity. The wave propagation speed varies with the properties of the ionosphere, troposphere. The necessary range corrections are supplied by the primary data products and are added to the range estimate, namely:

- the ionosphere correction,
- the dry troposphere correction, and
- the wet troposphere correction.

In addition to atmospheric corrections, the range is corrected to account for sea level changes due to tides and atmospheric pressure, using the following correction parameters:

- dynamic atmosphere correction,
- elastic ocean tide,
- long-period ocean tide,

- ocean loading tide,
- solid earth tide, and
- geocentric polar tide.

The final step is then to compute the surface elevation relative to the WGS84 ellipsoid, obtained by subtracting the retrieved range from the altitude of the satellite.

5.5 Sea-Surface Height and Freeboard

5.5.1 Sea-Surface Height

The estimation of the instantaneous sea-surface height (*SSH*) along the trajectory is computed by implementing a series of steps:

1. Elimination of major sea-level changes caused by geoid and mean dynamic topography by subtracting a mean sea-surface elevation (DTU21, see auxiliary data section).
2. Smoothed interpolation between elevation tie points in leads and extrapolation to the full trajectory (sea level anomaly, *SLA*).
3. Uncertainty computation and filtering of *SLA* based on total number and distance to the next *SSH* tie point.

Generally written, *SSH* is defined as:

$$SSH = MSS + SLA$$

Where

MSS = the Mean Sea Surface, and

SLA = the Sea Level Anomaly.

5.5.2 Sea-Surface Height Uncertainty

The uncertainty of the sea-surface height depends on the base *SSH* uncertainty, and the distance to the closest sea-surface height tie point (e.g., the closest direct measurements of sea-surface height over open water between sea-ice floes). The values for base *SSH* uncertainty are assumed to be 2 cm to include effects such as leads covered with thin ice. The maximum uncertainty is assumed to be 10 cm, based on investigations of the typical variation of the anomaly between the instantaneous sea-surface height and mean sea surface along polar crossing orbits.

$$\sigma_{SSH} = \begin{cases} 0.02 \text{ m} + 0.1 \text{ m} \times \left(\frac{d_{tp}}{100 \text{ km}} \right)^2, & d_{tp} < 100 \text{ km} \\ 0.1 \text{ m}, & d_{tp} \geq 100 \text{ km} \end{cases}$$

Where

d_{tp} = the distance to the next sea-surface height tie point

5.5.3 Freeboard

Two definitions of freeboard are used:

1. Radar Freeboard: Residual between ice surface elevations and SSH without range corrections due to lower wave propagation speed in the snow layer.
2. Sea-Ice Freeboard: Residual between ice surface elevations and SSH with range corrections due to lower wave propagation speed in the snow layer.

The unit of radar and sea-ice freeboard, as well as snow depth, is meters. The distinction assumes that the retracked range represents the distance from the satellite to the snow/ice interface. However, this distance is computed with vacuum light speed, and a geometric correction needs to be applied for the slower wave propagation speed in the snow layer. Radar freeboard is therefore the residual between ice surface elevations and the sea-surface height (**Figure 5-7**):

$$rfrb = elev_{sea\ ice} - ssh$$

which is converted to sea-ice freeboard (frb) by using a correction factor (Δr_{wp}) dependent on snow depth (SD) and snow density (ρ_s):

$$frb = rfrb + \Delta r_{wp}$$

Where

$$\Delta r_{wp} = \left(\frac{c}{c_s} - 1 \right) \cdot sd$$

$$c_s = c \left(1 + 0.51 \times \rho_s \right)^{-1.5}$$

5.5.4 Freeboard Uncertainty

The radar freeboard uncertainty is computed by error propagation of the range or elevation uncertainty, and the sea-surface height uncertainty, and is given by:

$$\sigma_{rfrb} = \sqrt{\sigma_{elev}^2 + \sigma_{ssh}^2}$$

and for sea-ice freeboard:

$$\sigma_{frb} = \sqrt{(sd \times \sigma_{sd})^2 + \sigma_{rfrb}^2}$$

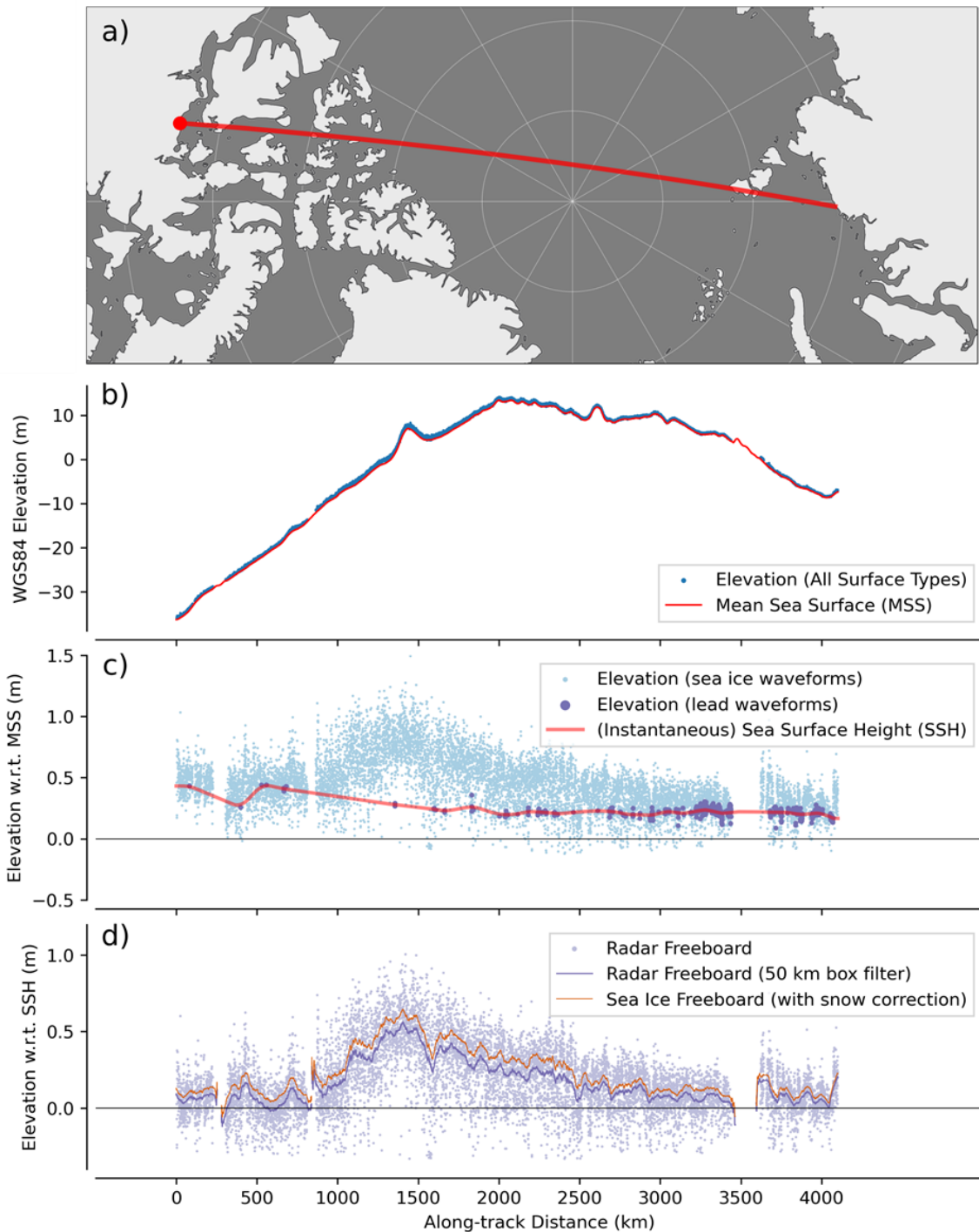


Figure 5-7: Example for the estimation of sea-ice freeboard for one CryoSat-2 orbit segment crossing the Arctic Ocean in April 2014. a) Location of orbit, red marker indicates start of orbit. b) Ellipsoidal (WGS84) elevation (ELEV) from all retracked

waveforms and mean sea-surface height (mss, here denoted in capitals). C) Elevations of all sea ice and lead elevation with respect to MSS with estimation of instantaneous sea-surface height (mss, here denoted in capitals) using lead tie points. d) Elevation of sea-ice waveforms with respect to the sea-surface height, defined as radar freeboard (*rfrb*). The running mean of radar freeboard, calculated using a 25 km box filter window, has been added to indicate average sea-ice freeboard at CDR grid resolution. Sea-ice freeboard (*frb*) is derived from radar freeboard points and elevation correction based on snow depth (*sd*) and density (ρ). Here, only the 50 km running mean of *frb* is shown.

5.6 Snow on Sea Ice

The sea-ice thickness retrieval from altimeter data critically depends on the knowledge of snow (depth and density) information. In absence of a basin-scale observational data set, we utilized climatological information from the Warren et al. 1999 (W99) snow climatology of Arctic sea ice in SICCI Phase 2. For the Arctic, this has been replaced with a merged climatology created by AWI. This new snow product merges the monthly Warren snow climatology with daily snow depth from AMSR2 data, provided by the Institute for Environmental Physics of the University Bremen, over first-year sea ice, creating monthly snow depth fields of snow depth and density parametrizations.

5.6.1 Snow Depth

For the merging of the two data sets, monthly composites of the AMSR2 snow depth fields are created to match the monthly resolution of the W99 climatology for the months from October to April. After that a Gaussian low pass filter with the size of 8 grid cells is applied on the AMSR2 snow depth composite, negative snow depths are removed and upper range limit is set to 60 cm. Then a regional weight factor w is created to ensure a smooth transition between the inner Arctic Basin domain and the area where AMSR2 is used. The merged snow depth (sd_{merged}) is computed as:

$$sd_{merged} = w \cdot sd_{W99} + (1 - w) \cdot sd_{AMSR2}$$

Figure 5-8 contains examples of the merging steps and **Figure 5-9** for the regional weight factor.

Following the common practice to modify the W99 snow climatology by reducing the values by 50% over first-year sea ice in the central Arctic (Tilling et al., 2018), the reduction is applied based on the ice type information for the particular orbit. This correction stems from Kurtz & Farrell (2011), which showed IceBridge measured snow thicknesses on FYI to be about 50% of the W99 estimates that are based on measurements made on MYI. Note that this scaling is applied only on the W99 snow, not on the AMSR2 snow depth. The scaled snow depth is:

$$c = (1 - f_{myi}) * c_{fyi} * w$$

$$sd = sd_{merged} - c \cdot sd_{merged}$$

Where $c_{fyi} = 0.5$ is the W99 scaling over first-year sea ice, c the total scaling factor including multiyear sea-ice fraction f_{myi} and the weight factor.

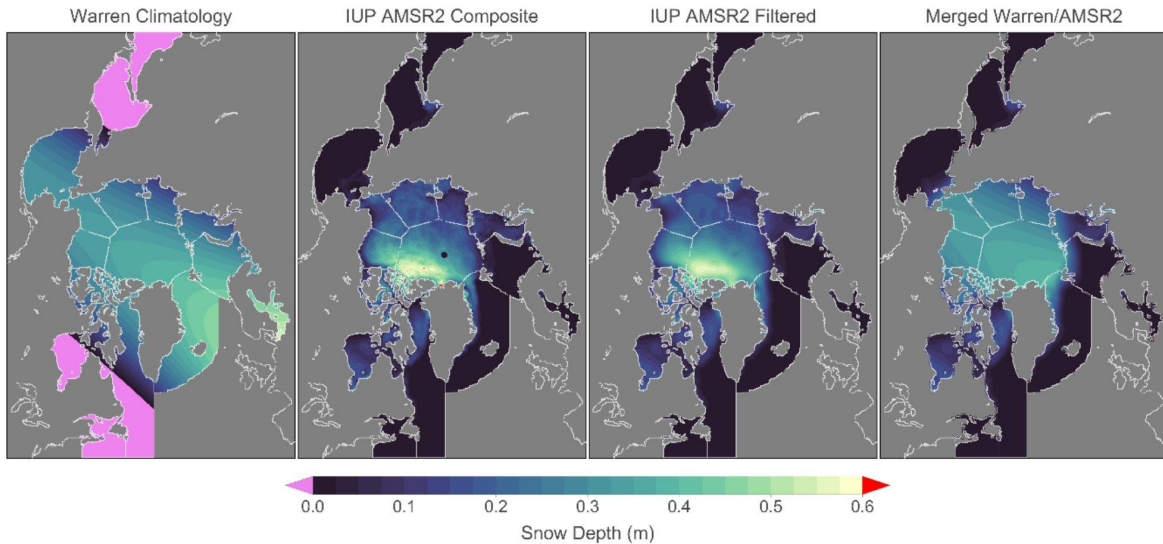


Figure 5-8: Steps for creating the monthly merged snow depth climatology. This example is for April, from left to right: 1) Warren snow depth climatology, 2) Monthly snow composite from daily AMSR2 data, 3) Low-pass filtered composite and 4) Merged Warren/AMSR2 with regional weight factor applied

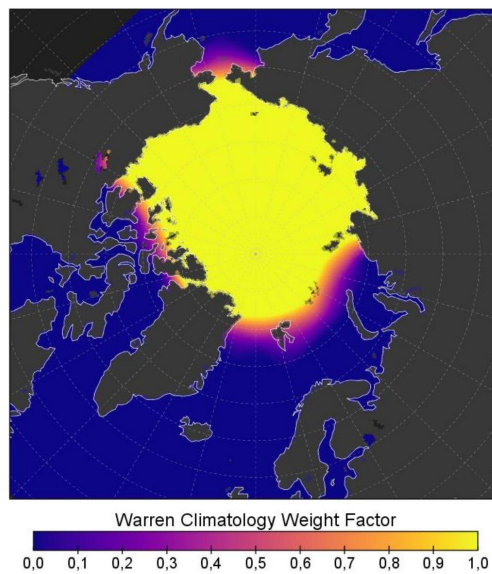


Figure 5-9: Regional weight factor for the W99 snow depth climatology

An example of the results with merged snow is in **Figure 5-10**. There are significantly less data gaps outside the central Arctic Basin, while retaining the W99 information on areas potentially covered with multiyear sea ice, areas where AMSR2 lacks sensitivity.

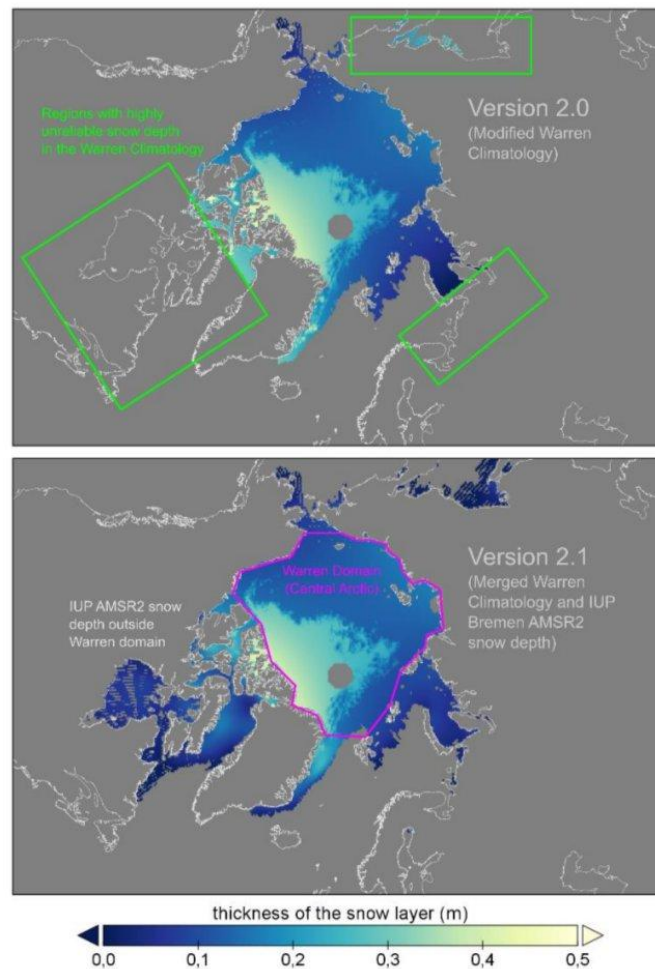


Figure 5-10: Performance example of sea-ice thickness with the merged W99/AMSR2 snow product. (Top) AWI CryoSat-2 v2.0 sea-ice product with W99 snow. (Bottom) sea-ice thickness with merged W99/AMSR2 snow depth climatology. The improvements are most drastic in areas outside the domain (marked with green rectangles) of the W99 climatology (marked with purple polygon)

Utilization of the monthly fields lead to unrealistic jumps in daily sea-ice freeboard and thickness values between the last day of a month and the first day of the next. Therefore, the monthly climatology is attributed to a reference day and linear interpolation is used between these days (**Table 5-5**).

The reference day for the monthly climatology is the center of the month except for October and April. The reference day for these months is set to be the beginning and end respectively, as the merged snow climatology does not exist for September and May and extrapolation proved unreliable.

The linear interpolation only affects the snow depth values before the ice-type based 50% correction.

Table 5-5: Reference dates for the monthly snow climatology used for the estimation of linear interpolated snow depth with daily resolution

Month	Oct	Nov	Dec	Jan	Feb	Mar
Reference Day	1.10.	15.11.	15.12.	15.1.	15.2.	30.3.

For the Antarctic, with only a single ice type, a simpler approach is taken by applying the AMSR-E/2 snow-depth climatology provided by the ICDC. The climatology is based on averages for each calendar day of the daily data, available at the ICDC University Hamburg: (<https://icdc.cen.uni-hamburg.de/en/esa-cci-sea-ice-ecv0.html>).

5.6.2 Snow Depth Uncertainty

The uncertainty of the merged snow depth is derived in a similar fashion. We merge the uncertainty provided by the W99 climatology and the AMSR2 snow depth using the regional weighting factor.

$$\sigma_{sd}^{merged} = w \cdot \sigma_{sd}^{W99} + (1 - w) \cdot \sigma_{sd}^{AMSR2}$$

The uncertainty of snow depth (sd) is represented as the scaled uncertainty plus an uncertainty term for the scaling itself:

$$\sigma_{sd} = \left(\sigma_{sd}^{merged} - c \cdot \sigma_{sd}^{merged} \right) + \left(sd \cdot c \cdot \sigma_{fyi} \cdot c_{fyi} \right)$$

In the Southern Hemisphere the field `mediansnowdepth_filtered100_variability` of the snow depth climatology product is used as an uncertainty estimate.

5.6.3 Snow Density

Here, we use a linear increasing snow density over the winter season following Mallett et al., 2020. This replaces using the average snow density in the central Arctic Basin in SICCI Phase-2. Similar to snow depth, the increase of snow density is computed with daily resolution.

$$p_s = 6.5 \times t + 274.51$$

With t representing the time in fractional month since October 15.

5.6.4 Snow Density Uncertainty

In the Arctic the snow density uncertainty (σ_{ρ}^s) is provided by the Warren climatology as well. The difference in sea-ice density between FYI and MYI is small, therefore the snow density and its uncertainty are assumed to be independent from the MYI fraction. In the Antarctic, we assume a fixed uncertainty of 20 kg/m³.

5.7 Sea-Ice Thickness

5.7.1 Freeboard to Thickness Conversion

The final step in the processing is to convert sea-ice freeboard to sea-ice thickness. The ice floe may or may not be covered by snow, but field studies have shown that if the floe is indeed snow-covered, the radar reflection and hence height measurement relate to the snow/ice interface. This however may not always be the case as was shown by the laser / radar altimeter study in Fram Strait during the RRDP exercise in CCI Phase 2. This most certainly is not the case for areas of seasonal sea ice, such as the Baltic Sea, for most of the winter. Thus freeboard values should be understood as "altimeter freeboard" values. That is, for the cold central Arctic they can be assumed to represent the ice freeboard, but for marginal areas the elevation measured is somewhere between the ice and snow freeboard. But since this effect cannot be parameterized with available EO data, it is always assumed in the processing that the dominant reflector is the snow/ice interface.

The conversion of sea-ice freeboard (frb) to sea-ice thickness (sit) requires the densities of sea ice (ρ_I), snow (ρ_s) and sea water (ρ_w) as well as snow depth as additional input parameters as follows:

$$sit = \frac{sd \times \rho_s - frb \times \rho_w}{\rho_w - \rho_I}$$

The sea-water density is assumed to be constant for the entire Arctic domain:

$$\rho_w = 1024.0 \frac{kg}{m^3}$$

while the snow density is taken directly from the original W99 climatology. The sea-ice density is assumed to be dependent on ice type, with the boundary conditions as the densities for FYI and MYI (Alexandrov et al., 2010):

$$\rho_I^{FYI} = 916.7 \frac{kg}{m^3}$$

$$\rho_I^{MYI} = 882.0 \frac{kg}{m^3}$$

The sea-ice density (ρ_I) is scaled with the sea-ice type/MYI area fraction (f_{MYI}) to account for the impact of surface type:

$$\rho_I = \rho_I^{FYI} - f_{MYI} \times (\rho_I^{FYI} - \rho_I^{MYI})$$

5.7.2 Sea-Ice Density Uncertainty

To estimate the uncertainty of the sea-ice density (σ_{ρ}^I), two terms are combined: 1) general density uncertainty scaled between the base uncertainties (Alexandrov et al., 2010) for FYI ($\sigma_{\rho}^{fyi} = 35.7 \frac{kg}{m^3}$) and MYI ($\sigma_{\rho}^{myi} = 23.0 \frac{kg}{m^3}$) density, and 2) a term for the scaling uncertainty:

$$\sigma_{\rho}^i = \underbrace{\sigma_{\rho}^{fyi} + f_{myi} \times (\sigma_{\rho}^{myi} - \sigma_{\rho}^{fyi})}_{\text{Base Uncertainty Scaling}} + \underbrace{\sigma_{f_{myi}} \times (\sigma_{\rho}^{fyi} - \sigma_{\rho}^{myi})}_{\text{Scaling Uncertainty}}$$

5.7.3 Sea-Ice Thickness Uncertainty

The SIT uncertainty (σ_{sit}) is then computed as the error propagation of all input uncertainties with the assumption that the sea-water density (ρ_w) is negligible:

$$\sigma_{sit} = \sqrt{\left(\frac{\rho_w}{\rho_w - \rho_i} \sigma_{frb}\right)^2 + \left(\frac{frb \cdot \rho_w + sd \cdot \rho_i}{\rho_w - \rho_i} \sigma_{\rho}^i\right)^2 + \left(\frac{\rho_s}{\rho_w - \rho_i} \sigma_{sd}\right)^2 + \left(\frac{sd}{\rho_w - \rho_i} \sigma_{\rho}^s\right)^2}$$

This error propagation is evaluated for every sea-ice thickness estimate of the Level-2 data.

5.7.4 Sea-Ice Type (MYI Fraction) Uncertainty

In the Arctic, the MYI fraction uncertainty ($\sigma_{f_{myi}}$) is taken directly from the MYI fraction product (field `my_sea_ice_area_fraction_sdev`)

No sea-ice-type product is available in the Antarctic and the general assumption is that all sea ice can be described as FYI. Nevertheless we assume a static uncertainty of 10% for the MYI fraction to account for sea-ice type based uncertainties.

5.8 Filtering

Filters for various parameters are used to remove erroneous or low-quality results for individual waveforms, or entire marine segments from the Level-2 output data. The action of each filter is logged in an error flag that is stored in the output data.

5.8.1 General Filters

Several filters are applied to the Level-2 based at various stages of the algorithm (**Table 5-6**)

Table 5-6: List of data filters for Level-2 processing of trajectory based radar altimeter data.

Filter	Criterion	Action
Lead tie points	No leads in marine areas enclosed by land. As a result, the sea-surface height in sea-ice covered areas may have a considerable bias.	Sea-surface height, radar as well as sea-ice freeboard and sea-ice thickness set to Not-a-Number (NaN) in marine areas enclosed by land.
Lead tie points (Envisat only)	Lead tie-point elevation (ELEV) is outside the envelope of local elevation range and likely subject to range bias. ELEV > mean + 2 standard deviations or ELEV < mean – 3 standard deviations Mean and standard deviation for one lead tie-point elevation is computed as a rolling parameter with a window size of 50 km. Standard deviation cannot be lower than 0.1 m.	Lead tie-point excluded from computation of sea level anomaly.
Lead tie points	Distance to next lead tie point > 200 km. This means the sea-surface anomaly is extrapolated from the last measurement and may have a considerable bias.	Sea-surface height, radar as well as sea-ice freeboard and sea-ice thickness set to Not-a-Number (NaN) for data points.
Sea-ice Freeboard	Removal of unrealistic sea-ice freeboard (<i>frb</i>) values, likely due to a waveform retracking issue. The filter includes a noise estimate which depends on the specific radar altimeter type. FRB < -0.25 m or FRB > 2.25 m (CryoSat-2) FRB < -0.5 m or FRB > 2.5 m (Envisat)	Sea-ice freeboard and thickness set to Not-a-Number (NaN).
Sea-ice thickness	Removal of unrealistic sea-ice thickness (SIT) values., likely due to a waveform retracking issue in combination with other factors that are not captured by the sea-ice freeboard filter. The filter includes a noise estimate which depends on the specific radar altimeter type. SIT < -0.5 m or SIT > 10.5 m (CryoSat-2) SIT < -1.0 m or SIT > 11.0 m (Envisat)	Sea-ice thickness set to Not-a-Number (NaN).

5.8.1 Marginal Ice Zone Filter

The marginal ice zone (MIZ), defined as the transitional zone between open ocean and dense sea ice, is subject to wave and swell penetration that influence radar altimeter waveform shape. The higher surface height variability by surface waves is, at the waveform level, ambiguous with the effect of thicker, rougher sea ice. Thus, the presence of surface waves in the MIZ results in a freeboard and ultimately sea-ice thickness bias. A filter is included in the SIT retrieval algorithm to automatically detect such events. The filter flag assumes three values (**Table 5-7**).

Table 5-7: Marginal ice zone (MIZ) filter flag values and meaning.

MIZ Filter Value	Flag Meaning
0	No MIZ
1	MIZ
2	MIZ and freeboard affected by wave/swell bias

There are two cases to be considered when detecting wave influence in MIZ based on the geometry of orbit and the sea-ice edge – open-ocean transitions to sea ice, and sea ice which is in proximity to the open ocean but is not in transition to open ocean.

5.8.1.1 Open-Ocean to Sea-Ice Transition

In this case, an orbit trajectory passes from open ocean into the sea-ice cover or vice versa. Multiple transitions per orbit segment are also possible. Each transition is detected, and the following computations are made per crossing:

1. Compute the distance to the ocean. This is done based on the gridded sea-ice concentration data, as the trajectory might run oblique to the ice edge. The distance to the ocean can only be computed with a granularity of the spatial resolution of the sea-ice concentration data.
2. Compute average leading-edge width (LEW) of open-ocean waveforms for the first 25 km of open water. LEW is a proxy for significant wave height.
3. Compute the sea-ice freeboard gradient with a smoothing window of 150 km.

The filter algorithm first estimates the likelihood of surface waves penetrating the sea-ice cover based on the properties of open ocean waveforms. Only if the open ocean LEW threshold is large enough, or a strong freeboard gradient in the ice cover is present, will the filter be active, and detect the impacted data based on behavior of sea-ice freeboard.

Filter settings have been adapted to the different sensitivities of Envisat/ERS and CryoSat-2 waveforms (**Table 5-8**).

Table 5-8: Marginal ice zone filter scheme for radar altimeter orbits that transit from open ocean into the sea-ice cover or vice versa. The output of the filter is the flag value that describes the presence of the marginal ice zone data (1) and very likely freeboard bias (2).

Flag Value	Envisat/ERS	CryoSat
1	Sea-Ice Waveforms within 300 km of open ocean (determined by sea-ice concentration)	
2	<i>Decision if swell event</i>	
	Open ocean LEW > 2.5 or Sea-ice-freeboard gradient at ice edge > 0.2 m/km	Open ocean LEW > 2.0 or Sea-ice-freeboard gradient at ice edge > 0.2 m/km
	<i>Find affected freeboard (only if swell event)</i>	
	From ice edge to first occurrence where sea-ice-freeboard gradient reaches 0 m/km	

5.8.1.2 Open-Ocean Proximity

There are cases where the freeboard is impacted by surface waves in the proximity of the ice edge, but the trajectory does not cross into open water. This case is not covered by the filter described in the previous section. An additional set of parameter thresholds is therefore used, that determine the MIZ flag value.

Filter settings have been adapted to the different sensitivities of Envisat/ERS and CryoSat-2 waveforms (**Table 5-9**).

Table 5-9: Marginal ice zone filter scheme for radar altimeter orbits that pass the marginal ice zone but do not cross into open ocean. The output of the filter is the flag value that describes the presence of the marginal ice zone data (1) and very likely freeboard bias (2).

Flag Value	Envisat/ERS	CryoSat-2
1	Sea-Ice Waveforms within 300 km of open ocean (determined by sea-ice concentration)	
2	<i>All conditions must be met</i>	

	Sea-Ice Concentration $\leq 75\%$	Sea-Ice Concentration $\leq 90\%$
	distance to low concentration sea ice (sea-ice concentration $\leq 70\%$) ≤ 200 km	distance to open ocean (sea-ice concentration $\leq 15\%$) ≤ 300 km
	Rolling mean of leading-edge width (25 km window) ≥ 1.0	Rolling mean of leading-edge width (25 km window) ≥ 2.0
	Rolling standard deviation (25 km window) of pulse peakiness ≤ 55.0	Rolling standard deviation (25 km window) of pulse peakiness ≤ 15.0

6 COLOCATION ON SPACE-TIME GRID (LEVEL-3 PROCESSOR)

Level-3 sea-ice thickness is processed by mapping the orbit-based Level-2 data onto a spatiotemporal grid. The temporal and spatial dimensions are described in the following subsections.

6.1 Grid Temporal Coverage

The data will be processed monthly for the winter season between October 1st and April 30th. Temporal specifics are described in Table 6-1:

Table 6-1: Temporal definition for Level-3 products.

	Monthly
Start of temporal coverage	First day of month 00:00:00 UTC
End of temporal coverage	Last day of month 23:59:59.999 UTC

6.2 Grid Spatial Definition

Data for both hemispheres will be gridded into the Equal-Area Scalable Earth Grid version 2 (EASE2-Grid) with 25 km resolution. The projection is defined in Table 6-2 and grid extent and spacing in the Level-3 product are defined in Table 6-3.

Table 6-2: Projection definition for Level-3 products.

Property	Hemisphere	Value
false_easting	North/South	0.0

false_northing	North/South	0.0
grid_mapping_name	North/South	lamber_azimuthal_equal_area
inverse_flattening	North/South	298.257223563
latitude_of_projection_origin	North	90.0
	South	-90.0
longitude_of_projection_origin	North/South	0.0
proj4_string	North	+proj=laea +lon_0=0 +datum=WGS84 +ellps=WGS84 +lat_0=90.0
	South	+proj=laea +lon_0=0 +datum=WGS84 +ellps=WGS84 +lat_0=-90.0
semi_major_axis	North/South	6378137.0

Table 6-3: Grid extent and spacing for Level-3 products.

Property	Value
Grid Dimension	(432, 432)
Grid Spacing (km)	25.0
Grid Notation	Center Coordinates
Grid x extent in projection coordinates (km)	(-5387.5, 5387.5)
Grid y extent in projection coordinates (km)	(-5387.5, 5387.5)

6.3 Parameter Gridding

Level-3 processing will grid Level-2 intermediate (I2i) files. All the Level-2 data points within the specific timeframe are transformed into projection coordinates and assigned an index of a corresponding grid cell in the target grid. Each target grid cell will then possess a dedicated parameter stack that contains all the geophysical variables from Level-2 data that were associated with that specific cell. There is no filtering applied at this stage, except for radar freeboard, where freeboard values in leads need to be set as NaN in the Level-3 processor. The parameter stack of Level-2 data ($p_{i,L2}$) is used to compute the gridded parameter geophysical value p_{L3} as an arithmetic mean, ignoring non-numeric values:

$$p_{L3} = \frac{1}{n_{L2}} \cdot \sum_{i=0}^{n_{L2}} p_{i,L2} \quad \text{if } p_{i,L2} \neq NaN$$

The geophysical parameters that will undergo gridding are:

1. radar freeboard
2. freeboard

3. sea-ice thickness
4. snow depth
5. snow density
6. sea-ice density
7. sea-ice type
8. sea-ice concentration

6.4 Level-3 Gridded Uncertainties

The Level-3 product contains the average uncertainties for freeboard/thickness respectively per grid cell to reflect that the biggest uncertainty components, e.g. snow depth, sea-ice density, retracker biases, are not random uncertainties that would be reduced by averaging, examples in Figure 6-1. The uncertainties of the gridded radar freeboard, freeboard and sea-ice thickness are therefore computed again with the error propagation functions, only that we use the weighted mean error for uncertainties of random variables (radar freeboard) and the average uncertainty from the orbit data for variables with systematic error components (snow depth, sea ice and snow density). This approach introduced in CCI+ results in a more realistic uncertainty magnitude compared to the SIT CRDP v2.0.

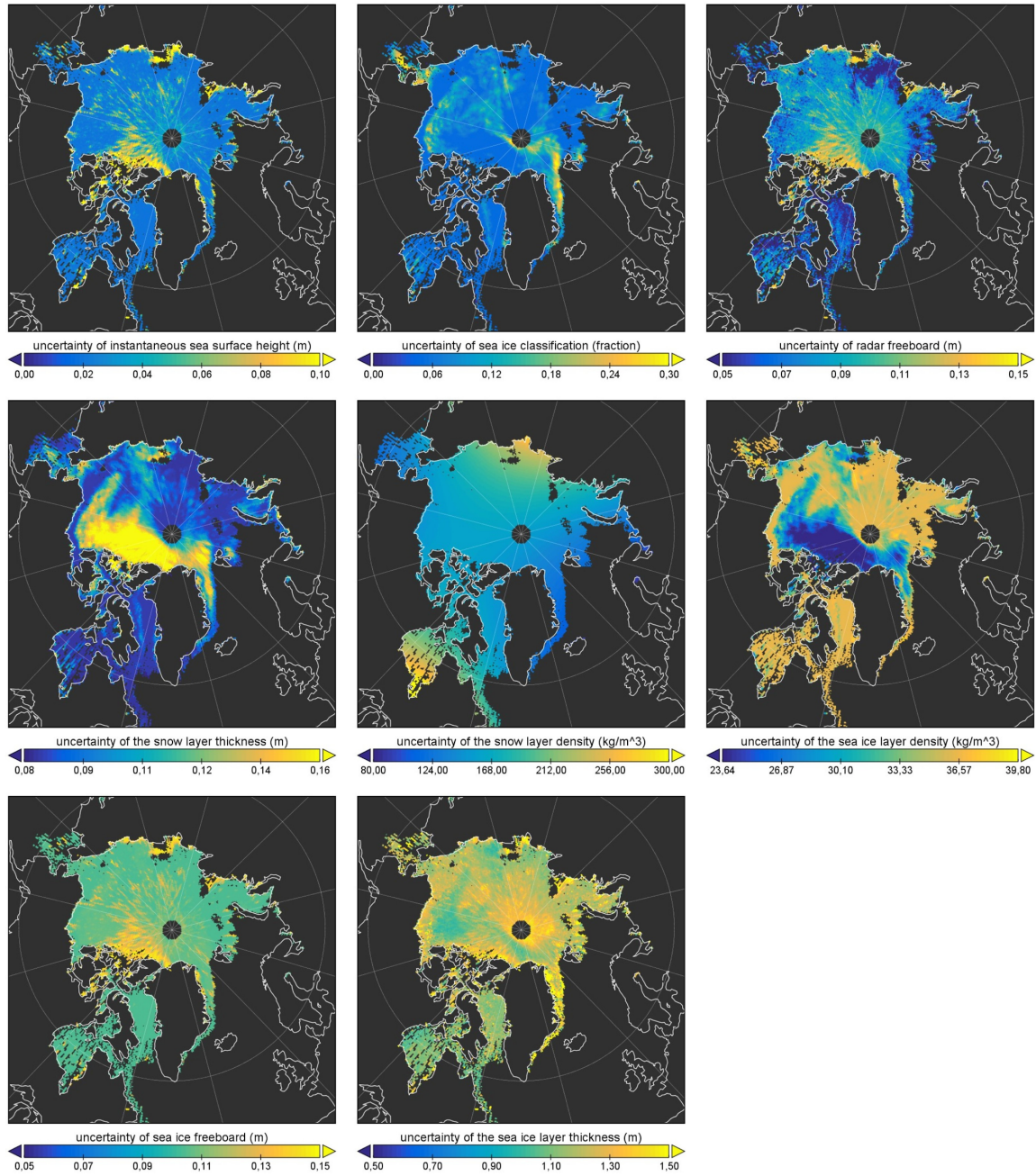


Figure 6-1: Gridded uncertainties (Example CryoSat-2 March 2015 Arctic data)

7 GAP INTERPOLATION (LEVEL-4 PROCESSOR)

Generally, the Level-4 data sets are created from lower level data which contains gaps due to lack of data coverage within the target period. Specifically, the Level-4 processor ingests sea-ice concentration data to determine where sea-ice thickness information needs to be available and computes an analysis of the available sea-ice thickness information from one or multiple platforms from Level-2 (trajectories) and Level-3 (space-time grids) data.

Areas that profit from the L4 product generation comprise the central Arctic basin “covered” by pole hole, the marginal seas with reduced spatiotemporal coverage, as well as topographical difficult areas such as the Canadian Archipelago. However, appropriate auxiliary data and methods are needed and tailored towards the specific regional challenges such as artifacts in the auxiliary data (e.g. from sea-ice concentration data) or varying interpolation window sizes.

Level-4 sea-ice thickness information for the ERS-1/2 and Envisat platforms in the Northern Hemisphere will rely on interpolation over significant distances, as these systems provide data only up to 81.5 deg north. As shown in Figure 7-1, at least the spatiotemporal evolution and variability within the Arctic Basin in- and outside the pole-hole area are rather consistent and co-varying.

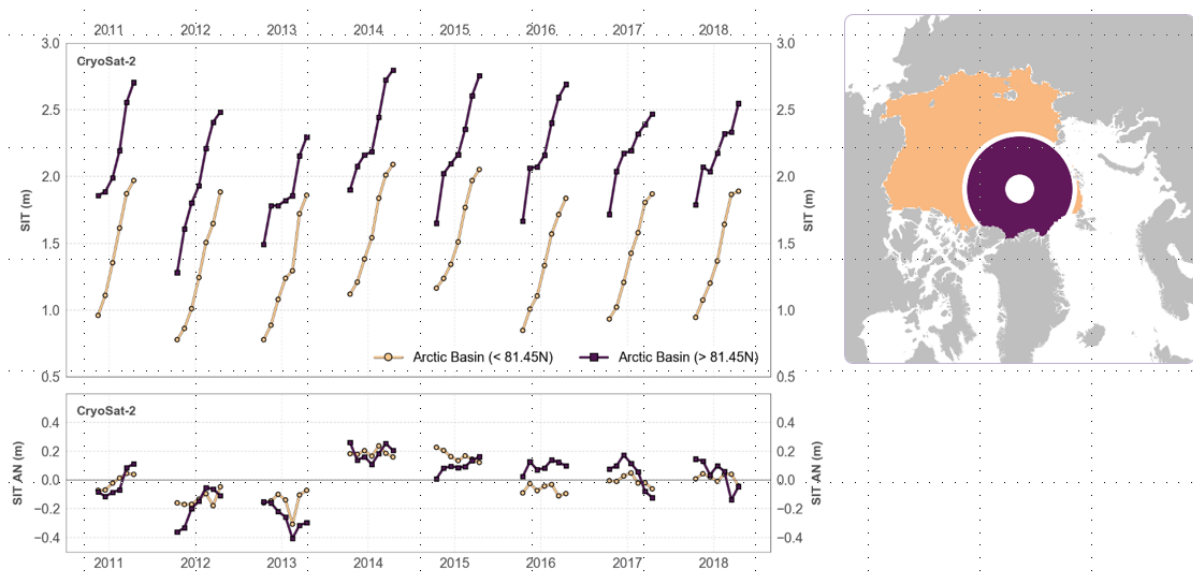


Figure 7-1: Evaluation of CryoSat-2 SIT area averages and their anomalies

A suitable metric guiding the interpolation process using optimal interpolation could be the *distance along iceline* (DAL; Lavergne et al., 2019; Figure 7-2), as well as CCI+ sea-ice concentration data as background.

Results from and an analysis of the finalized Level-4 processor will be available in future versions of this document.

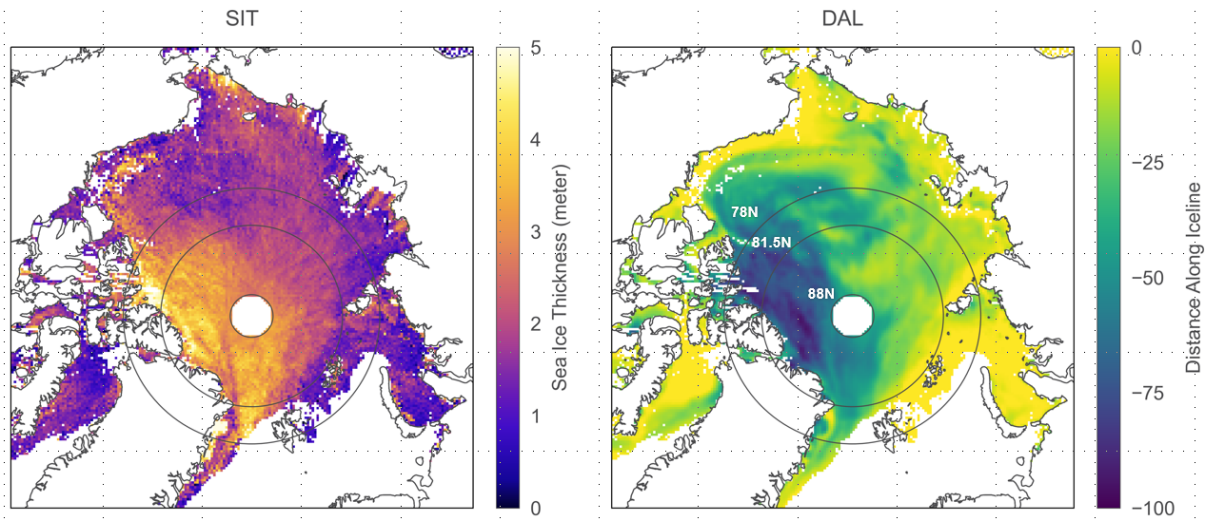


Figure 7-2: CryoSat-2 SIT (left); Distance along iceline (DAL; right) for April 2016.

8 SEA-ICE VOLUME COMPUTATION

For volume calculation, the individual sea-ice thickness measurements are coupled with ice concentration values (C3S, Table 2-1). This is done using the gridded Level-4 product as gap-free data and its corresponding area (i.e., the area of a grid cell) is needed. Volume is calculated only where ice concentration is above 15%, so an ice extent mask is applied to rule out areas outside the 15% concentration. Sea-ice volume is then the sum product of sea-ice thickness, concentration as well as the cell marine area of all grid cells covered.

$$SIV = \sum_{i=0}^n SIT_i \cdot SIC_i \cdot A_i^{marine}$$

The input for the marine area per grid cell is a dedicated land mask developed in CCI based on high resolution coastline data and generated for the target grid. The land mask is shared between all sea ice ECV variables. The mask contains the fraction of all grid cells covered by ocean domains and the marine fraction is then derived by multiplying this fraction with grid cell area (25 km²). The marine fraction is independent from the ice-covered fraction of the grid cell, which is provided by the sea-ice concentration product.

This section is to be extended and completed. The finalized section including uncertainty computation will be available with the data at the end of Phase 2 of CCI+.

9 REFERENCES

Brockley, D. J., Baker, S., Féménias, P., Martínez, B., Massmann, F-H., Otten, M., Paul, F., Picard, B., Prandi, P., Roca, M., Rudenko, S., Scharroo, R., and Visser, P.: REAPER: Reprocessing 12 Years of ERS-1 and ERS-2 Altimeters and Microwave Radiometer Data, IEEE TGRS, doi: 10.1109/TGRS.2017.2709343, 2017.

Cavalieri, D. J., Markus, T., and Comiso, J. C. 2014. AMSR-E/Aqua Daily L3 12.5 km Brightness Temperature, Sea Ice Concentration, & Snow Depth Polar Grids. Version 3. June 2002 – October 2011. Boulder, Colorado USA: NASA National Snow and Ice Data Center Distributed Active Archive Center. doi: http://dx.doi.org/10.5067/AMSR-E/AE_SI12.003.

European Space Agency, 2018, RA-2 Sensor and Geophysical Data Record - SGDR. Version 3.0, <https://doi.org/10.5270/EN1-85m0a7b>

European Space Agency, Fundamental Data Records for Altimetry: Detailed Processing Model CLS-ENV-NT-20-0424, 2021.

Helm, V., Humbert, A., and Miller, H. (2014) Elevation and elevation change of Greenland and Antarctica derived from CryoSat-2, *The Cryosphere*, 8, 1539-1559, <https://doi.org/10.5194/tc-8-1539-2014>.

Kurtz N., Farrel SL.: Large-scale surveys of snow depth on Arctic sea ice from Operation IceBridge. *Geophysical Research Letters*, Vol. 38, L20505 2011. doi:10.1029/2011GL049216

Lavergne, T., Sørensen, A. M., Kern, S., Tonboe, R., Notz, D., Aaboe, S., Bell, L., Dybkjær, G., Eastwood, S., Gabarro, C., Heygster, G., Killie, M. A., Brandt Kreiner, M., Lavelle, J., Saldo, R., Sandven, S., and Pedersen, L. T.: Version 2 of the EUMETSAT OSI SAF and ESA CCI sea-ice concentration climate data records, *The Cryosphere*, 13, 49–78, <https://doi.org/10.5194/tc-13-49-2019>, 2019.

Laxon, S. W., Peacock, N. R. & Smith, D. M. (2003) High interannual variability of sea ice thickness in the Arctic region. *Nature*, doi:10.1038/nature2050, 947-950.

Mallett, R. D. C., Lawrence, I. R., Stroeve, J. C., Landy, J. C., and Tsamados, M.: Brief communication: Conventional assumptions involving the speed of radar waves in snow introduce systematic underestimates to sea ice thickness and seasonal growth rate estimates, *The Cryosphere*, 14, 251–260, <https://doi.org/10.5194/tc-14-251-2020>, 2020.

Paul, S. & Hendricks, S.: Feed-Forward Neural Network for ENVISAT Retracker Threshold Computation (v1.0), Zenodo. <https://doi.org/10.5281/zenodo.7436473>, 2022.

Paul, S. & Hendricks, S.: Feed-Forward Neural Network for ERS-2 Retracker Threshold Computation (v1.0), Zenodo. <https://doi.org/10.5281/zenodo.8335298>, 2023.

Peacock, N. R. (1998) Arctic sea ice and ocean topography from satellite altimetry, Ph.D. thesis, University College London.

Peacock, N. R. & Laxon, S. W. (2004) Sea surface height determination in the Arctic Ocean from ERS altimetry. *Journal of Geophysical Research*, Vol. 109, No. C7, C07001 10.1029/2001JC001026.

Ricker, R., Hendricks, S., Helm, V., Skourup, H., and Davidson, M. (2014) Sensitivity of CryoSat-2 Arctic sea-ice freeboard and thickness on radar-waveform interpretation, *The Cryosphere*, 8, 1607-1622, doi:10.5194/tc-8-1607-2014.

Tilling, R, Ridout, A., Shepherd, A.: Estimating Arctic sea ice thickness and volume using CryoSat-2 radar altimeter data. *Advances in Space Research*, Volume 62, Issue 6, 15 September 2018, Pages 1203-1225, doi: <https://doi.org/10.1016/j.asr.2017.10.051>

Warren, S. G., Rigor, I. G., Untersteiner, N., Radionov, V. F., Bryazgin, N. N., Aleksandrov, Y. I., and Colony, R. (1999) Snow depth on Arctic sea ice, *J. Climate*, 12, 1814–1829.